TU Delft

Delft University of Technology

Document Version
Final published version

Licence
CC BY-NC-ND

Citation (APA)
Novelli, V. I., Freddi, F., Whitworth, M., Stokes, M., Belfoul, A., Esper, S., Feldbrugge, M., Giardina, G., Foroughnia, F., & More Authors (2026). The 2023 M_w 6.8 Al Haouz, Morocco earthquake: A multi-layer reconnaissance framework for the remote sensing and field assessment of landslides, building and heritage damage, and road access disruption in the High Atlas region. *International Journal of Disaster Risk Reduction*, *145*, Article 106400. https://doi.org/10.1016/j.ijdrr.2026.106400

Important note
To cite this publication, please use the final published version (if applicable).
Please check the document version above.

Copyright
In case the licence states “Dutch Copyright Act (Article 25fa)”, this publication was made available Green Open Access via the TU Delft Institutional Repository pursuant to Dutch Copyright Act (Article 25fa, the Taverne amendment). This provision does not affect copyright ownership.
Unless copyright is transferred by contract or statute, it remains with the copyright holder.

Sharing and reuse
Other than for strictly personal use, it is not permitted to download, forward or distribute the text or part of it, without the consent of the author(s) and/or copyright holder(s), unless the work is under an open content license such as Creative Commons.

Takedown policy
Please contact us and provide details if you believe this document breaches copyrights.
We will remove access to the work immediately and investigate your claim.

This work is downloaded from Delft University of Technology.

International Journal of Disaster Risk Reduction 145 (2026) 106400



Contents lists available at ScienceDirect

International Journal of Disaster Risk Reduction

journal homepage: www.elsevier.com/locate/ijdrr

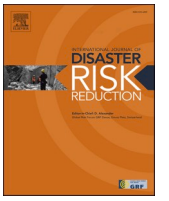

The 2023 M_w 6.8 Al Haouz, Morocco earthquake: A multi-layer reconnaissance framework for the remote sensing and field assessment of landslides, building and heritage damage, and road access disruption in the High Atlas region

Viviana Iris Novelli [a,*], Fabio Freddi [b], Michael Whitworth [c], Martin Stokes [d], Alaeddine Belfoul [e], Sarah Esper [a], Riccardo Vitale [f], Zeyad Khalil [g,h], Mauritz Feldbrugge [i], Asmaa Maaroufi [j], Hiba Shaimed [k], Hamza Skikra [l], Alejandra Albuerne [m,n], Marco Redaeli [o], Giorgia Giardina [i], Keith Adams [p], Roberto Gentile [q], Siau Chen Chian [r], Sarah J. Boulton [d], Joshua Jones [c], Pietro Milillo [f,s,t], Fatemeh Foroughnia [i], Valentina Putrino [u], Jacob Black [v]

[a] *Department of Civil Engineering, Cardiff University, UK*
[b] *Department of Civil, Environmental and Geomatic Engineering, University College London, UK*
[c] *Aecom, UK*
[d] *School of Geography, Earth and Environmental Sciences, University of Plymouth, UK*
[e] *University Ibn Zohr, Morocco*
[f] *Department of Civil and Environmental Engineering, Cullen College of Engineering, University of Houston, Houston, TX, USA*
[g] *Department of Civil and Environmental Engineering, Imperial College, UK*
[h] *Department of Civil and Environmental Engineering, The Hong Kong Polytechnic University, Hong Kong*
[i] *Department of Geoscience and Engineering, Delft University of Technology, The Netherlands, the Netherlands*
[j] *School of Collective Intelligence, University Mohammed VI Polytechnic, Morocco*
[k] *Global Diversity Foundation, Morocco*
[l] *Geology and Sustainable Mining Institute, University Mohammed VI Polytechnic, Morocco*
[m] *ISchool of Architecture & Design, IE University, Spain*
[n] *Bartlett School of Architecture, University College London, UK*
[o] *Gruner Italia S.r.l., Italy*
[p] *School of Engineering & Design, College of Technology & Environment, London South Bank University, UK*
[q] *Department of Disaster Risk Reduction, University College London, UK*
[r] *National University of Singapore, Singapore*
[s] *Department of Earth and Atmospheric Science, Cullen College of Engineering, University of Houston, Houston, TX, USA*
[t] *Microwaves and Radar Institute, German Aerospace Center DLR, Weßling, Germany*
[u] *Ariel Re UK Limited, UK*
[v] *Civic, UK*

ARTICLE INFO

Keywords:
Earthquake reconnaissance
Remote sensing
Earthquake-induced landslides

ABSTRACT

On 8 September 2023, a M_w 6.8 earthquake struck Morocco's High Atlas region, causing nearly 3000 fatalities and widespread damage across rural, mountainous settlements dominated by traditional and non-engineered construction, and affecting cultural heritage assets. The event triggered landslides that further increased the isolation of affected communities. This study

* Corresponding author.
E-mail address: novelliv@cardiff.ac.uk (V.I. Novelli).

https://doi.org/10.1016/j.ijdrr.2026.106400
Received 27 May 2026; Received in revised form 25 August 2026; Accepted 25 August 2026
Available online 31 August 2026
2212-4209/© 2026 Published by Elsevier Ltd. This is an open access article under the CC BY-NC-ND license (http://creativecommons.org/licenses/by-nc-nd/4.0/).

Building damage assessment
Multi-layer geospatial framework
Multi-hazard assessment
Mountainous regions

presents findings from the Earthquake Engineering Field Investigation Team (EEFIT) mission. Different radar and optical remote sensing techniques were used to identify areas most affected by earthquake-induced landslides and building damage, guiding the field investigations. A total of 2671 earthquake-induced landslides were identified; although relatively limited for an event of this magnitude, they significantly impacted road accessibility and emergency response. In parallel, 455 buildings were assessed on site and classified using the EMS–98 scale. Seismic performance was primarily influenced by construction practices and detailing rather than structural typology. Traditional unreinforced masonry buildings exhibited the highest vulnerability, largely due to substandard materials and construction practices, and limited upkeep, which are common in remote villages. Hybrid constructions combining traditional and modern techniques also performed poorly. Confined masonry and reinforced concrete buildings generally performed better, although deficiencies in detailing and irregular configurations were frequently observed. Cultural heritage assets sustained predominantly moderate damage, and stabilisation efforts are ongoing. By combining remote sensing and systematic engineering field observations within a common geospatial framework, the study presents a multi-layer reconnaissance framework for interpreting landslide inventories, building damage, and cultural heritage observations together in data-scarce mountainous regions, while highlighting priorities for future research and practice.

1. Introduction

On 8 September 2023 at 22:11 local time, a moment magnitude (M_w) 6.8 earthquake struck Morocco's High Atlas Mountains [1], causing 2960 fatalities, 5600 injuries, and the damage or destruction of over 50,000 housing units [2]. The most severe impacts were concentrated in Al Haouz Province, extending westward into Chichaoua, southward into Taroudant, and towards Ouarzazate and urban areas such as Marrakesh. Fig. 1 shows the spatial distribution of the event, while Fig. 2 provides a few representative examples of earthquake impacts. The mainshock was followed by a relatively limited aftershock sequence. Only two aftershocks exceeded the routine cataloguing threshold (M_w 4.5) of the U.S. Geological Survey National Earthquake Information Center (NEIC) [1]: an M_w 4.9 event occurring approximately 20 min after the mainshock and an M_w 4.6 event on 14 September 2023 (see Fig. 1). NEIC also reported three additional lower–magnitude events (one M_w 4.0 and two M_w 4.2); however, no further events met the publication criteria due to the limited availability of arrival-time observations. As a result, the aftershock dataset remains sparse and does not provide sufficient constraints to further refine the geometry of the causative fault(s) [3,4].

The most affected areas were characterised by dispersed mountain settlements situated along steep slopes, often built from locally sourced materials and using traditional techniques (Fig. 2a). However, impacts were also observed in urban centres further from the

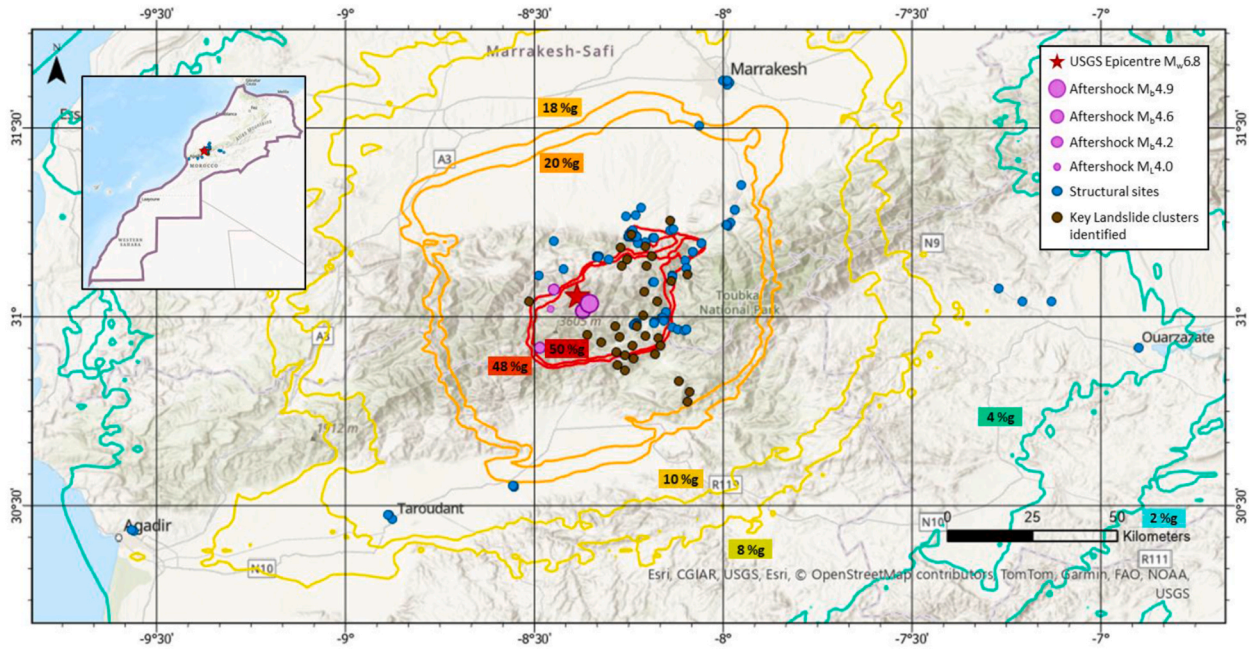

Fig. 1. Locations of the main event and aftershocks, peak ground acceleration (PGA) contours (%g) from the U.S. Geological Survey (USGS) [5–7], and sites inspected during the field mission. Note: M_b = Body Wave Magnitude; M_L = Local Magnitude; M_w = Moment Magnitude. The inset shows the location of the earthquake epicentre in relation to Morocco's national administrative boundary.

epicentre, including Marrakesh. The earthquake produced severe social and economic consequences, with total losses estimated at $8–11 billion and a national reconstruction programme of approximately $11.7 billion announced by the Moroccan government [2,8]. Widespread destruction of residential buildings was reported, particularly in remote communities where non-engineered constructions are common, resulting in extensive partial and total collapses (Fig. 2b). The event also triggered numerous landslides, which damaged and blocked roads and electricity infrastructure, further isolating mountain settlements (Fig. 2c) [9–11]. In addition, significant impacts were recorded on Morocco's built cultural heritage, including 27 protected monuments such as the UNESCO World Heritage sites of the Medina of Marrakech and the Aït Ben Haddou *ksar*, as well as the Tinmel Mosque, listed on the UNESCO Tentative List [5–7]. This event highlighted the vulnerability of mountainous regions, where strong ground shaking interacts with steep terrain, triggering secondary hazards such as landslides. This combination amplifies impacts and complicates both emergency response and post-earthquake damage assessment (Fig. 2d).

Following the earthquake, Moroccan authorities and international organisations mobilised extensive emergency response operations involving civil protection agencies, armed forces, and humanitarian organisations [12–16]. In parallel, the Government of Morocco, supported by the World Bank, the European Union, and the United Nations, undertook a Post-Disaster Needs Assessment (PDNA) to quantify the physical, social, and economic impacts of the earthquake and identify priorities for recovery and resilient reconstruction [17]. Concurrently, scientific teams conducted rapid engineering reconnaissance, remote sensing (RS) analyses, and field investigations to support damage assessment, including building damage classification, the identification of predominant construction typologies, and mapping of earthquake-induced landslides [18–25]. Building on these governmental and scientific assessment activities, numerous studies have subsequently investigated the seismotectonic characteristics of the earthquake, ground motion patterns, RS products, and engineering performance of the affected building stock.

Although Morocco lies within a complex tectonic setting related to the convergence of the African and Eurasian plates, strong earthquakes are relatively uncommon in the High Atlas Mountains, and the region remains underrepresented in global ground–motion databases. Consequently, several studies have examined the seismotectonic context, rupture processes, and ground–motion characteristics of the event [26–29]. RS, including optical satellite imagery and Synthetic Aperture Radar (SAR) techniques, has also been widely used to support damage detection and analysis of co–seismic ground deformation following the 2023 Morocco earthquake [30–35].

Building on previous RS and field-based reconnaissance studies of the 2023 Al Haouz earthquake, and on the Earthquake Engineering Field Investigation Team (EEFIT)'s international experience, including missions in Sumatra (2009) [36], Nepal (2015) [37],



Fig. 2. Earthquake impacts in the High Atlas region: (a) overview of Imi N'Tala Al Haouz Province (High Atlas Mountains), showing a typical mountain settlement with dense construction along steep slopes; (b) extensive collapse of residential buildings in Imi N'Tala, constructed with non-engineered techniques in remote communities; (c) earthquake-triggered rockfalls and landslides along the Tizi N'Test corridor, obstructing mountain roads and requiring clearance operations; and (d) collapse of hillside dwellings in Talat N'Yaaqoub, illustrating the interaction between steep terrain and structural vulnerability.

Albania (2019) [38], Haiti (2021) [39], Turkey (2023) [40], this study extends previous investigations that have primarily examined individual aspects of the event, such as seismotectonic processes, RS analyses, or building damage. It does so by developing a spatially consistent, multi-layer post-earthquake framework in which complementary RS products and systematic field observations are organised within a common geospatial environment. Specifically, the study: (i) uses complementary RS techniques to identify and prioritise areas for detailed field reconnaissance; (ii) develops a systematic inventory of landslides, including earthquake-induced landslides (EQLs), from high-resolution satellite imagery, refined through field observations, and relates their spatial distribution to road accessibility and the observed impacts on affected communities; (iii) undertakes a systematic georeferenced assessment of residential and non-residential buildings using European Macroseismic Scale (EMS–98) damage classifications, linking building typology, construction characteristics, observed damage, and failure mechanisms within a common spatial framework; and (iv) assesses damaged designated cultural heritage assets, documenting their construction characteristics, pre-earthquake state of conservation, observed damage, emergency stabilisation measures, and conservation interventions alongside their cultural and socio-economic significance. The novelty of the study does not lie in the individual datasets themselves, but in their combined use within a common spatial framework. Rather than focusing on a single aspect of the earthquake, the framework brings together regional RS, landslide mapping, engineering assessments of buildings, and cultural heritage investigations, enabling relationships between hazards, accessibility disruption, structural performance, and heritage impacts to be interpreted across regional, settlement, and asset scales. This provides a more comprehensive understanding of the earthquake than would be possible from any individual dataset alone.

This study follows a four-phase reconnaissance workflow (Section 2). Following an overview of the seismological context of the event (Section 3), the pre-field phase provides a regional-scale screening of earthquake impacts using RS, focusing on landslides (Section 4.1) and building damage (Section 5.1). This is followed by field and post-field analyses that draw upon the complementary thematic layers organised within the common geospatial framework to examine landslides and road disruption (Section 4.2), building damage and structural performance (Section 5.2–5.4), and impacts on cultural heritage (Section 6). Although the results are presented in thematic sections corresponding to the principal reconnaissance components, their interpretation is informed by complementary observations from the remaining thematic layers, enabling regional RS-derived disturbance patterns to be examined alongside detailed engineering evidence collected during the field reconnaissance. This common spatial framework supports a coherent multi-scale interpretation of the earthquake impacts and their implications for reconstruction priorities, future risk reduction, and context-specific recommendations.

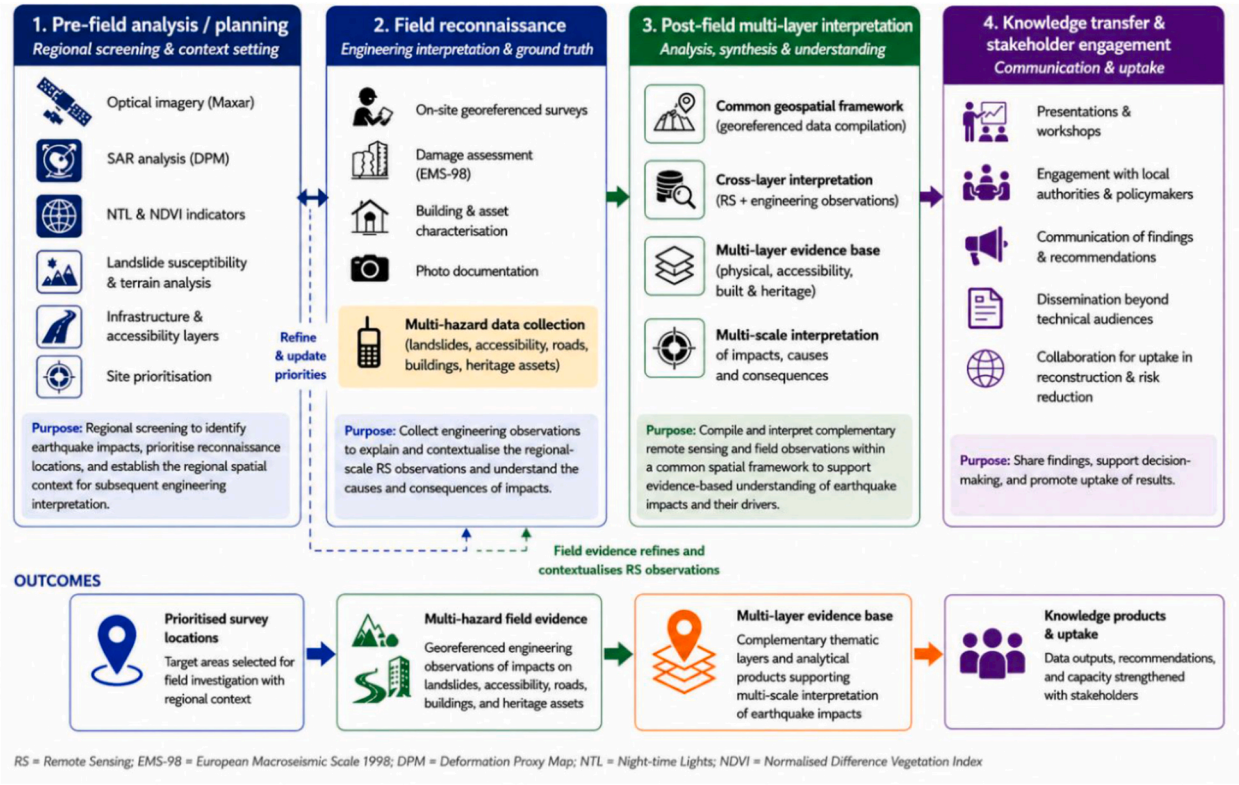

Fig. 3. Multi-layer reconnaissance and post-earthquake assessment framework.

2. Mission structure and methodological approach

The EEFIT reconnaissance approach follows a structured four-phase workflow comprising: (1) pre-field analysis/planning, (2) field reconnaissance, (3) post-field multi-layer interpretation, and (4) knowledge transfer and stakeholder engagement (Fig. 3). The pre-field stage uses complementary RS products to provide a regional screening of earthquake impacts and prioritise reconnaissance locations. The field reconnaissance stage collects systematic georeferenced engineering observations of landslides, roads, buildings, infrastructure, and cultural heritage. The post-field stage brings together RS products and field observations within a common geospatial framework, enabling complementary datasets to be interpreted together while retaining their individual thematic purpose. Finally, the knowledge-transfer stage supports dissemination of the findings and engagement with stakeholders to inform reconstruction and disaster risk reduction.

2.1. Pre-field analysis/planning

Since the early 2000s, EEFIT has integrated RS in post-earthquake assessment missions [39–42]. This approach has evolved into a hybrid operational model in which remote analysts and field teams collaborate, enabling continuous exchange of data throughout the reconnaissance process. Within this multi-hazard reconnaissance framework, this phase focused on identifying the areas most affected by the earthquake and providing a rapid regional overview to support field mission planning.

High-resolution optical imagery (*e.g.,* Maxar Open Data) was first used to identify and map landslides, providing an initial regional assessment of their spatial distribution. Beyond establishing a preliminary EQL inventory, this analysis identified areas where slope failures were likely to affect the principal mountain transport corridors, highlighting locations where road access could be disrupted and where field access might be constrained. This information was used to support reconnaissance planning, optimise field routes, and identify priority areas for subsequent ground verification.

In parallel, SAR-based Damage Proxy Maps (DPMs), Nighttime Light (NTL) analysis, and Normalised Difference Vegetation Index (NDVI) filtering were used to identify settlements with potential building damage. The complementary RS products, including the preliminary landslide inventory, DPMs, and reductions in NTL intensity, were interpreted jointly by the reconnaissance team to prioritise settlements exhibiting the strongest overall evidence of earthquake disturbance. The prioritisation did not rely on predefined thresholds or a formal weighted scoring system. Instead, the survey plan was refined by considering road accessibility, safety and logistical constraints, while deliberately including additional settlements representing different damage levels and geological settings to broaden the geographical coverage of the survey and reduce potential bias towards the most severely affected or most accessible locations. This strategy provided broad spatial coverage of the affected region and a robust basis for subsequent field reconnaissance and integration of field observations with regional-scale RS analyses.

The pre-field analysis is designed to be undertaken immediately following an earthquake, as soon as suitable RS data become available. The interval between completion of the pre-field analysis and field deployment depends not only on operational, logistical, and administrative constraints, but also on the timing and availability of suitable datasets for the specific event. Consequently, the workflow is intended to support, rather than replace, official post-earthquake reconnaissance and damage assessment activities by supporting reconnaissance planning and the efficient allocation of field resources.

This phase also included mission planning activities, such as team selection, coordination with local institutions, and logistical preparation.

2.2. Field reconnaissance

The field reconnaissance phase built upon the pre-field RS analysis by collecting the engineering observations required to refine, interpret, and contextualise the regional-scale RS observations within the common multi-layer assessment framework. Rather than functioning as an independent survey, the field investigations provided the engineering evidence necessary to explain the regional disturbance patterns identified during the pre-field analysis.

The principal field mission was conducted in April–May 2024 in the priority areas identified during the pre-field planning phase (Fig. 1). Although the RS analysis was completed shortly after the earthquake, deployment of the international field team was delayed by governmental authorisations and logistical considerations, including the Ramadan period. These constraints affected the timing of the deployment but not the reconnaissance strategy or the selection of the priority survey locations. A follow-up mission in December 2024 was undertaken to verify selected observations, document post-earthquake interventions, and collect supplementary information where required.

Landslides were systematically investigated to refine the preliminary RS mapping. Field observations documented landslide location, failure type (*e.g.,* rockfall, slide, topple), approximate dimensions, lithological setting, runout characteristics, and impacts on terrain and infrastructure. Attention was given to road blockages, transport corridors, and evidence of repeated clearance operations, providing information on post-earthquake road accessibility and the identification of accessible and isolated settlements. All field observations were georeferenced and linked to photographic records.

Within each district selected during the pre-field analysis, contiguous (agglomerated or clustered) groups of buildings along accessible roads were systematically surveyed. Where possible, all visible buildings within each survey unit were assessed. Consequently, the number of buildings surveyed in each settlement varied according to settlement size, the extent of the accessible built area, and field accessibility rather than a predetermined sample size. Surveying complete groups of adjacent buildings is standard practice in post-earthquake reconnaissance [43–45], as it minimises selection bias, including the tendency to preferentially inspect the most

severely damaged buildings, thereby providing a more representative assessment of earthquake performance across the surveyed area.

Although national housing statistics are available for Morocco through the 2024 High Commission for Planning (HCP) census [46], they classify buildings primarily according to construction materials and housing characteristics rather than structural typologies. Furthermore, Morocco's seismic regulations [47] do not provide an engineering-based classification of existing buildings. These limitations are particularly relevant in the High Atlas region, where mixed construction techniques and incremental modifications are common, making the engineering classification of existing buildings more challenging. Accordingly, a bespoke digital survey form was developed using Google Forms to systematically document the structural typology, construction materials, roof and floor systems, number of storeys, observed failure mechanisms, EMS–98 damage classification [48], and georeferenced photographic documentation for each surveyed building. Unlike conventional reconnaissance forms based on predefined building categories, the survey form was designed to capture mixed construction materials, hybrid structural systems, structural irregularities, and other vulnerability characteristics through structured fields and free-text observations. The same survey protocol was applied to non-residential buildings, including schools, healthcare facilities, religious buildings, commercial premises, hotels, and industrial facilities.

Designated cultural heritage assets of monumental character were surveyed within the areas selected for the field campaign, where previous reports and local information indicated earthquake damage. Buildings sharing the same traditional construction techniques, but without formal heritage designation, were assessed using the standard building survey described above. For each monument, the survey documented construction materials, structural typology, structural and non-structural damage, dominant failure mechanisms, emergency stabilisation measures, the pre-earthquake state of conservation, evidence of previous conservation interventions, and georeferenced photographic records. Damage was classified using the EMS–98 damage grades [48], while its interpretation considered the construction characteristics, conservation condition and heritage significance of each asset. The objective was not to produce a comprehensive inventory of all damaged heritage assets, but to document representative monuments exhibiting different construction techniques, damage levels, and post-earthquake conservation responses.

As the field surveys were undertaken several months after the earthquake, some sites had already undergone debris removal, emergency stabilisation, road clearance, demolition, or partial reconstruction. Where these post-earthquake interventions were observed, they were documented during the reconnaissance and considered when interpreting the observed earthquake damage.

2.3. Post-field multi-layer interpretation

Following the field campaign, all RS outputs and field observations were compiled within a common GIS environment to create a spatially consistent, multi-layer post-earthquake dataset. All datasets were referenced to a common coordinate system, enabling complementary information collected at regional, settlement, and building scales to be visualised, compared, and interpreted within a common spatial framework. Georeferenced field observations were linked to photographic documentation to support interpretation, verification, and traceability.

The dataset was organised into five complementary thematic layers, each addressing a different aspect of the earthquake impacts. While each layer can be analysed independently according to its specific objectives, their co-location within a common GIS environment enables observations from one layer to provide spatial and engineering context for interpreting the others. Together, the layers support a more comprehensive understanding of earthquake impacts than would be possible from any individual dataset alone. (i) **A regional RS layer** containing the pre-field DPM, NTL, NDVI, and preliminary landslide products. This layer provided the regional context for the field campaign by identifying areas exhibiting different levels of earthquake impact together with relative road accessibility, supporting the prioritisation and selection of reconnaissance locations. (ii) **A landslide layer** documenting the mapped landslide inventory identified during field reconnaissance, including geological and geomorphological characteristics and associated impacts. The combination of remotely mapped and field-validated observations enabled the distinction between earthquake-triggered and pre-existing landslides and improved the interpretation of the geological and geomorphological controls governing landslide occurrence, susceptibility, and associated impacts on road accessibility, buildings, and infrastructure. (iii) **A residential building layer** containing structural typology, construction characteristics, EMS–98 damage classifications, and observed failure mechanisms, enabling the interpretation of relationships between construction characteristics and observed damage, the identification of the most vulnerable construction typologies, and the preliminary identification of factors influencing differences in seismic performance within and between reconnaissance locations. (iv) **A non-residential building layer** containing equivalent structural and damage information for schools, healthcare facilities, commercial buildings, mosques, and other public infrastructure, supporting the interpretation of earthquake impacts on critical facilities. (v) **A cultural heritage layer** documenting construction characteristic, pre-earthquake state of conservation and past interventions, damage classifications, observed failure mechanisms, and emergency stabilisation measures for surveyed heritage assets, enabling the interpretation of heritage vulnerability and priorities for conservation and post-earthquake recovery.

The complementary nature of the thematic layers enables observations to be interpreted in relation to one another. The regional RS layer provides the spatial context for field observations, the landslide layer explains variations in accessibility and local hazard conditions, the residential and non-residential building layers relate these conditions to structural performance and community functionality, and the cultural heritage layer extends the assessment to historically significant assets. Considered together within a common spatial framework, these layers provide a more complete interpretation of earthquake impacts across regional, settlement, and asset scales than could be achieved through any single layer alone. Together with ancillary datasets, including regional ShakeMap ground motion estimates, these complementary layers support a more comprehensive interpretation of earthquake impacts across regional, settlement, and asset scales, while allowing each thematic layer to retain its specific purpose and level of detail.

This common spatial framework underpins the analyses presented in Sections 4–6. Although each section focuses primarily on one

or more thematic layers, the shared GIS environment enables the findings to be interpreted alongside complementary observations from the remaining layers, supporting a coherent multi-scale understanding of the earthquake impacts.

2.4. *Knowledge transfer and stakeholder engagement*

As a final stage of the reconnaissance workflow, knowledge transfer and stakeholder engagement were undertaken to support the dissemination of results and facilitate exchange with stakeholders. This phase included a dedicated workshop held in May 2025 at Mohammed VI Polytechnic University (UM6P) in Benguerir, Morocco, organised in collaboration with local partners, including researchers, technical experts, practitioners, and policymakers. The workshop provided a structured platform to discuss preliminary observations from the mission in relation to local needs and priorities. Discussions were organised around key themes, including seismic hazard characterisation, performance of traditional and non-engineered construction, landslide impacts, and post-earthquake reconstruction. The exchanges were consistent with observations from the field investigations and analyses presented in this study, particularly regarding challenges related to compliance with seismic codes, the need for context-specific damage classification approaches, and limitations in available geophysical and geotechnical data for hazard assessment. Discussions also addressed the importance of open-access, centralised geospatial databases and emphasised the need to align data collection and integration efforts with stakeholder requirements to support a multi-hazard risk assessment and informed decision-making. This stage complements the technical workflow by linking field-derived observations with broader considerations for reconstruction, data sharing, and future risk reduction. While the conclusions of this study are grounded in the proposed multi-layer reconnaissance framework, stakeholder engagement provided additional context for identifying practical needs and implementation pathways. A detailed description of the workshop objectives, programme, activities, and outcomes has been published separately [49]. Within the context of the present study, the workshop served to contextualise the reconnaissance findings in relation to national reconstruction priorities, practical implementation challenges, and stakeholder perspectives. The evidence-based recommendations presented in the Conclusions (Section 7) are informed by both the multi-layer assessment developed in this study and the outcomes of these stakeholder discussions.

3. Seismology

Although Morocco exhibits a lower seismic activity compared to other Mediterranean regions, its seismic hazard remains significant, as demonstrated by destructive events such as the 1960 Agadir earthquake (~12,000 fatalities) and the 2004 Al Hoceima earthquake (629 fatalities). Seismicity in Morocco is primarily linked to the ongoing convergence between the African and Eurasian plates, occurring at rates of approximately 4–8 mm/year. Despite extensive cataloguing efforts (*e.g.,* Cherkaoui & El Hassani, 2012 [50], documenting ~25,000 events between 1901 and 2010), the mechanisms controlling earthquake distribution and frequency remain poorly understood. Morocco's tectonic framework is complex, comprising four principal geological domains: the Precambrian Anti–Atlas, the Hercynian Meseta, the Atlas intracontinental belts, and the Rif Alpine belt. These domains are separated by major fault systems, with additional internal strike–slip faults contributing to structural complexity. Regionally, seismicity is concentrated in the

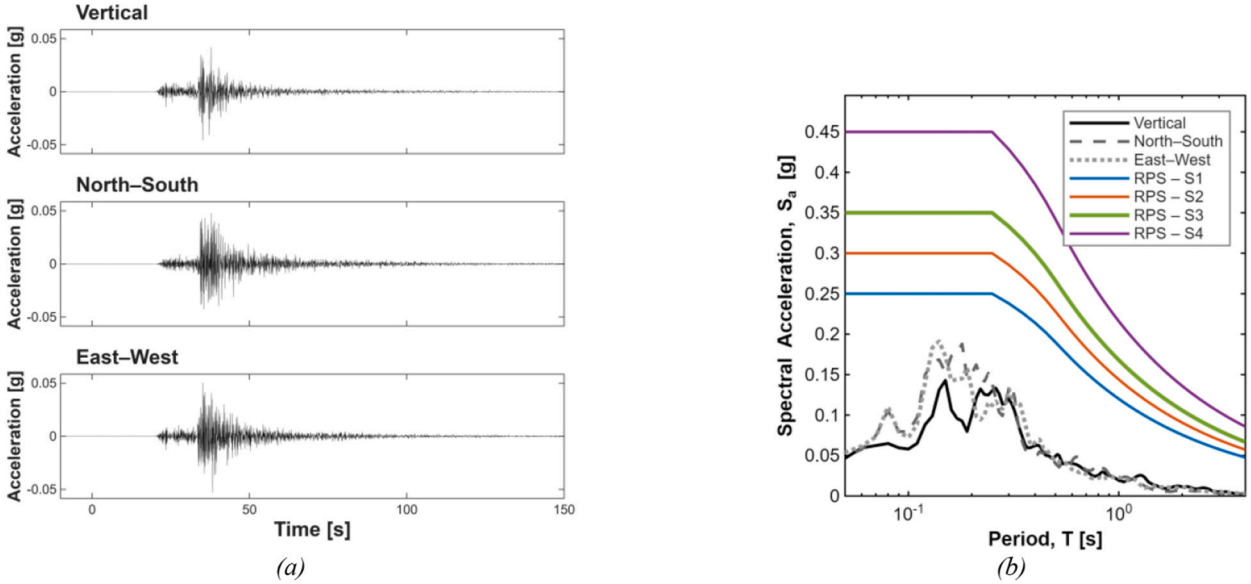

Fig. 4. (a) Three-component acceleration time histories recorded at the ROA/UCM/GEOFON Tiouine station (Code: WM.TIO; Location: 30.93° N, 7.26° W; Elevation: 1335 m), approximately 100 km from the epicentre, during the Mw 6.8 Al Haouz earthquake (8 September 2023, 22:11 local time) [53]. (b) Corresponding acceleration response spectra compared with the Moroccan seismic code (RPS 2000 [47]) design spectra for site classes S1–S4.

Rif domain (notably Al Hoceima), the Western Rif (NW–SE alignment), and the Atlas domain. The Atlas Mountains, comprising the Middle and High Atlas, represent an intraplate setting that continues to accommodate Africa–Eurasia convergence. Deformation is expressed through thick–skinned thrusting and folding within a double–vergent mountain belt structure. Major tectonic features include the North Atlas Fault (NAF) and South Atlas Fault (SAF), both associated with historical seismicity, including the 1960 Agadir event [51].

The 8 September 2023 M_w 6.8 Al Haouz earthquake occurred in the High Atlas, approximately 550 km south of the plate boundary, within a region of relatively low historical seismicity. The event was generated by oblique–reverse faulting in the lower crust (15–35 km depth), without surface rupture, indicating activation of a blind fault. Two main source models have been proposed: (i) a steep north–dipping fault linked to the Tizi n'Test structure, and (ii) a moderately south–dipping fault associated with the NAF. Current evidence favours the latter, involving dip slip (up to ~2.2 m) on a low-angle thrust [52]. Fig. 4 shows the three-component acceleration time histories recorded at the Tiouine (TIO) station, located approximately 100 km away from the epicentre [53], together with the corresponding response spectrum. Tiouine is one of the very few seismic stations available in Morocco and is in Zone 2 of the 2011 version Moriconi seismic code (RPS2000), corresponding to a design PGA of 0.1g for 475-year return period [47]. The recorded PGA in Tiouine was ≈0.05g (Fig. 4a), while the peak spectral acceleration reached ≈0.19g (Fig. 4b). However, the absence of instrumental stations in the near-source region limits the direct characterisation of ground shaking close to the epicentre and the ability to establish robust correlations between recorded motions and the observed damage [54]. The earthquake sequence included several aftershocks with magnitudes up to Mb 4.9 [1]. Despite its larger magnitude, the mainshock caused less catastrophic damage than the 1960 Agadir earthquake because of its greater focal depth and distance from major urban centres. Fig. 1 shows the USGS ShakeMap estimates, indicating PGA values of approximately 0.4–0.5g across the surveyed area, with lower values in peripheral zones [1]. These estimates provide valuable regional context but are subject to uncertainty because they are derived from sparse instrumental observations in the High Atlas region. Furthermore, uncertainty in local site response, including topographic amplification and valley (basin) effects, cannot be adequately characterised because of the lack of detailed site characterisation and reliable Vs,30 maps. These limitations should be considered when interpreting the relationship between the estimated PGA values and the observed damage patterns.

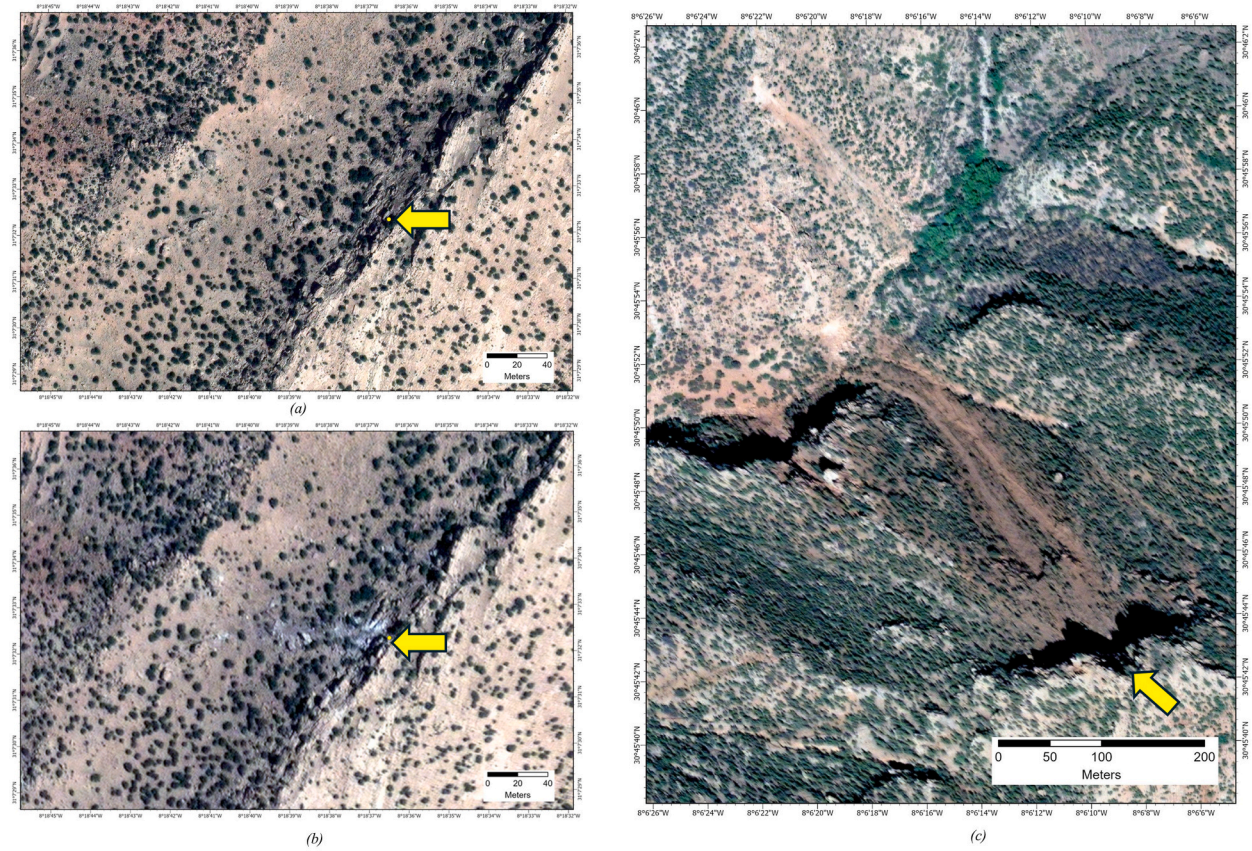

Fig. 5. Maxar satellite image examples of rockfalls triggered by the September 2023 Al Haouz earthquake. (a–b) Pre– and post–event imagery illustrating a typical, difficult–to–identify small–scale cliff failure in Mesozoic limestone. (c) Rare large–scale cliff failure rockfall of Mesozoic limestone with long runout.

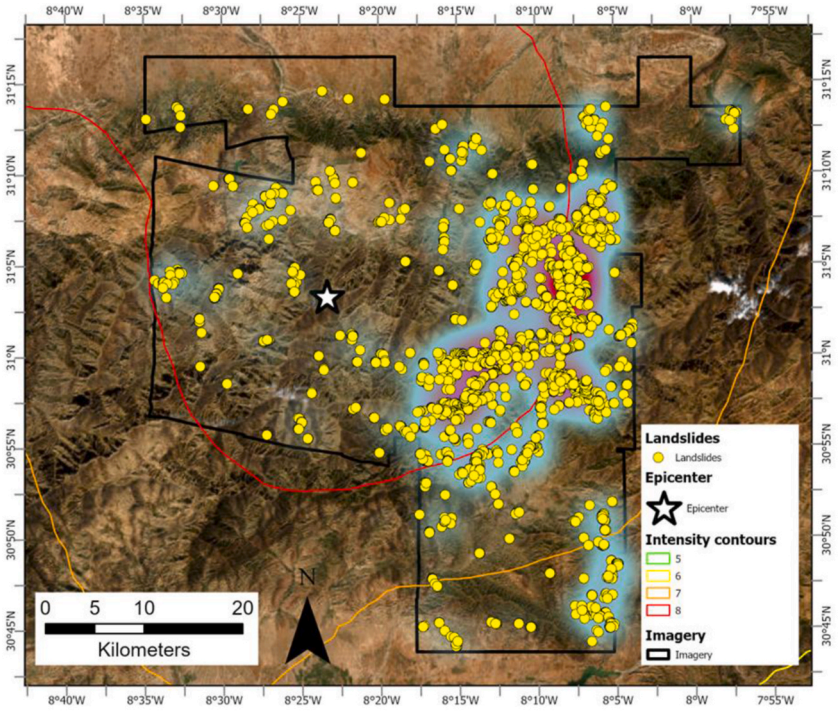

(a)

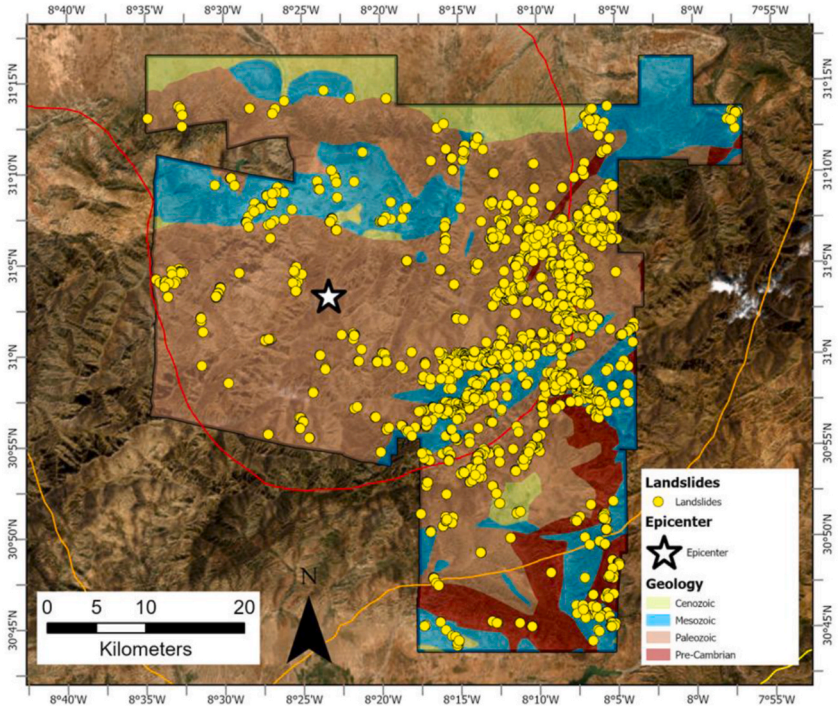

(b)

Fig. 6. Spatial distribution of the mapped landslides identified from the remote sensing analysis in relation to (a) the USGS ShakeMap Modified Mercalli Intensity (MMI) contours and the location of the 8 September 2023 Mw 6.8 Al Haouz earthquake epicentre, and (b) the regional geological units and the earthquake epicentre. The black polygons indicate the extent of the high-resolution optical imagery used for the landslide mapping.

4. Earthquake–induced landslide (EQLs) and road access disruption: observations and geotechnical assessment

4.1. Spatial analysis of landslides and road access disruption (Pre–Field)

A range of RS techniques was evaluated during the EEFIT Mission to provide a first-order regional assessment of landslide occurrence. EQLs represent a major secondary hazard associated with seismic events, often exceeding the direct impacts of ground shaking in terms of damage, fatalities, and infrastructure disruption. Events such as the 2018 Hokkaido [55] and the 2015 Gorkha [56] earthquakes demonstrate the scale at which EQLs can occur, highlighting their importance in hazard assessment and disaster response.

The 2023 Al Haouz earthquake in Morocco provides a further case study of the significant role of landslides in shaping post–earthquake impacts, particularly in mountainous regions such as the High Atlas. The earthquake–affected area of the High Atlas presents a complex geological and geomorphological setting that strongly influences landslide occurrence. Unlike many seismically active mountain belts, the High Atlas is in an intraplate setting, several hundred kilometres from the primary Africa–Europe plate boundary in the Mediterranean to the north. As a result, earthquake activity, and consequently earthquake–triggered landsliding, is relatively infrequent.

The region comprises a Precambrian crystalline basement overlain by Palaeozoic, Mesozoic, and Cenozoic sedimentary sequences, deformed into a fold–thrust belt with numerous reactivated tectonic structures. These structures, including the Tizi n' Test fault system associated with the Al Haouz earthquake, play a critical role in controlling slope stability by introducing discontinuities within rock masses. Lithologically, the study area is dominated by Palaeozoic quartzites and schists, Mesozoic sandstones and limestones, and Quaternary alluvial deposits. These materials exhibit varying mechanical properties that influence landslide style and distribution. Stronger lithologies, such as quartzites and limestones, tend to produce blocky rockfalls, whereas weaker materials, such as schists and unconsolidated soils, are more prone to shallow slide failures. Topographically, the High Atlas is characterised by steep slopes (25° mean), high relief (exceeding 3000 m), and deeply incised river valleys reaching hundreds of metres in depth [57].

A range of RS techniques were evaluated during the EEFIT Mission, including SAR and high–resolution optical imagery. However, the SAR data was characterised by a relatively coarse spatial resolution (10 m), limiting its effectiveness in detecting small–sized EQLs. Additionally, similarities in radar backscatter between landslide scars and surrounding terrain further complicated detection. In contrast, high–resolution optical imagery from the Maxar Open Data Program proved more effective for detailed landslide mapping. With a spatial resolution of approximately 0.3 m, these data allowed for visual identification of changes in terrain, vegetation, and surface characteristics (Fig. 5). Due to limitations in automated classification—caused by image distortions, small landslide size, and sparse vegetation cover—manual interpretation of pre– and post–event imagery across a 2400 km^2 area encompassing the earthquake epicentre and its highest intensity ground shaking (Modified Mercalli Intensity (MMI) VIII–V) was employed (Fig. 5).

Fig. 6 represents the landslide layer of the common multi-layer post-earthquake dataset. Although only the mapped landslides are displayed, each georeferenced observation is combined within the common database to detailed field information, including landslide classification, dimensions, lithological setting, runout characteristics, and impacts on roads and surrounding infrastructure. This multi-layer approach enables the mapped landslides and the identified EQLs to be interpreted alongside road access disruption, building



Fig. 7. Earthquake landslide field examples. (a) Mesozoic limestone rockfall with long runout; (b) Mesozoic limestone debris partially blocking the road; (c) Palaeozoic schist rockfalls/slides and soil slide debris runouts; (d) Soil slide failures of Quaternary River terrace sediments.

damage, geological conditions, and the complementary RS products within a common spatial framework. This approach resulted in the identification of 2671 landslides that were predominantly classified as shallow translational slides and rockfalls, with rarer deep-–seated failures (Fig. 7). Landslides were mainly concentrated 15–30 km E and SE of the epicentre along the large Oued N'Fis river valley within the zone affected by very strong (MMI = VIII) ground shaking. The Oued n'Fis, is one of the main river systems of the central (Marrakech) High Atlas that exploits the Tizi n'Test shear zone, a network of faults whose rupture initiated the Al Haouz event and its aftershocks. Importantly, this valley also contains the principal mountain transport corridors linking numerous remote settlements. Consequently, the spatial concentration of EQLs within this corridor provides regional-scale information on the areas, most susceptible to road disruption, highlighting where road blockages and restricted access to mountain communities were most likely to occur following the earthquake. These accessibility constraints have important implications for emergency response, the delivery of humanitarian assistance, and the prioritisation of post-earthquake reconnaissance in remote mountainous environments.

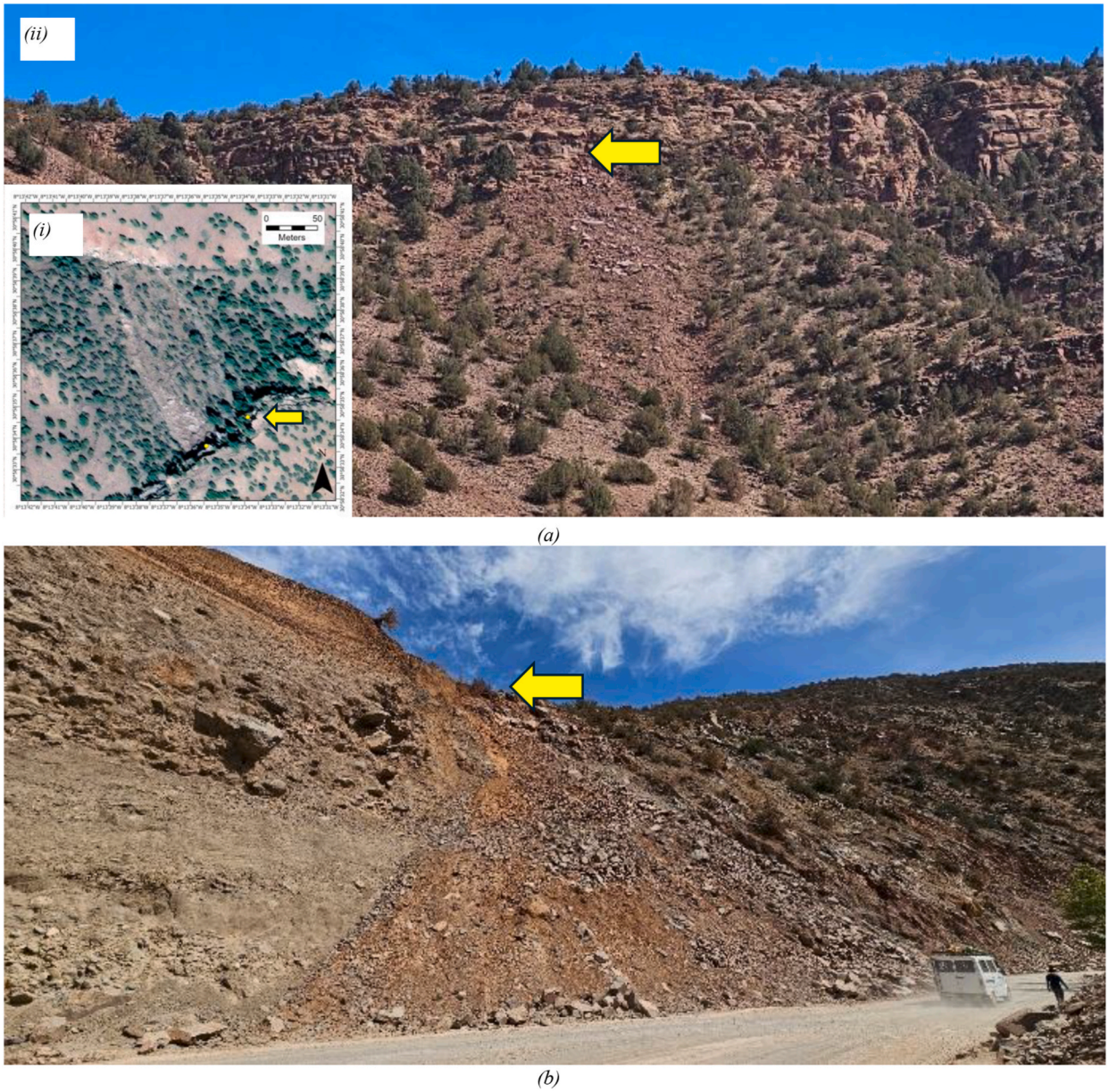

Fig. 8. (a) Mesozoic sandstone rockfall initiated from the ridgeline cliff: (i) Maxar satellite image; (ii) Field image, and (b) R202/N7 road widening near Imgdal village, with failure of Palaeozoic schist and Quaternary soil cut slope, resulting in road blockage and clearing. The failure has reactivated multiple times since the initial failure and clearing.

4.2. Field observations and Earthquake–Induced landslide (EQLs) and road access disruption

A spatial framework was developed to provide a regional-scale screening of earthquake impacts across the affected area. Rockfalls were the most common failure type, occurring predominantly in both Palaeozoic metamorphic rocks and Mesozoic sedimentary units. In Palaeozoic quartzite–schist terrains, closely spaced discontinuities facilitated rockslides with fragmentation into smaller blocks (<1 m) and granular material. In contrast, Mesozoic sandstone and limestone terrains comprised wider spaced discontinuities of bedding and joints. This facilitated rockfalls and topples that comprised larger–scale blocks (>1 m). Landslide debris sometimes occurred as runout across valley floors, as blocks and granular debris, or as localised debris cones along the main river channel margins. However, landslide runouts were frequently channelised, with debris often stored within the hillslopes. This slope–sediment storage configuration presents remobilisation hazards, especially if future low frequency–high magnitude dryland flash floods or wetter winter conditions are experienced. In addition to rockfalls, failures in unconsolidated coarse–gravel soils were observed, particularly along Quaternary River and fan terraces. These failures were typically shallow and associated with pre–existing erosional features such as gullies, indicating that seismic shaking reactivated geomorphologically conditioned slopes. Such processes highlight the importance of antecedent landscape evolution in determining landslide susceptibility.

RS and field observations following the earthquake revealed that most landslides were initiated along slope breaks such as ridgelines and cliffs. Rockfalls, topples, and shallow debris slides were the dominant failure types. In many cases, initial small m–scale rockfalls fragmented into granular material that travelled downslope through pre–existing hillslope channel networks, often with limited runout distances (~10's m) and small area coverages (~10–100's m^2) (Fig. 8a). Anthropogenic factors also contributed significantly to the occurrence and impacts of landslides. Road infrastructure, particularly along the R203/N7 highway, was widely affected by landslides (Fig. 8b). Failures were commonly associated with road cuttings, slope undercutting, and engineered slopes, which introduced additional instability. In some cases, large road-blocking landslides associated with Palaeozoic schists occurred in areas undergoing road widening reconstruction, demonstrating the interaction between human activity and natural hazard processes. Blockage of roads by landslide debris, often comprising large boulders of Mesozoic sandstone or limestone, significantly impeded emergency response and recovery operations by restricting access to remote mountain communities, delaying search-and-rescue activities, the delivery of humanitarian assistance, and the mobilisation of engineering teams responsible for road clearance and post-earthquake damage assessment.

The results of the study highlighted that the Al Haouz Earthquake triggered landslides at the expected locations, primarily near the epicentre, and showed a strong influence of rock type, material strength, and slope geomorphology. Nevertheless, although 2671 landslides were documented across the 2400 km^2 study area (Fig. 6), this number can be considered low for a M_w 6.8 event, compared to predictions for this event [1] and to previous observations from other events, which triggered ~5000–10,000+ landslides [58,59]. The dryland climate setting likely accounts for this low number of EQLs, despite the steep mountain slopes and variable rock–soil strength. However, the concentration of landslides within the principal river valleys east and southeast of the epicentre is particularly significant because these valleys coincide with the principal transport corridors linking numerous mountain settlements. Consequently, although the overall number of mapped EQLs was relatively low for an earthquake of this magnitude, their spatial concentration increased the potential for repeated road blockages, restricting access to remote communities and delaying emergency response. This demonstrates that, in mountainous regions where settlements rely on a limited number of valley roads, relatively localised landsliding can have disproportionate consequences for road accessibility and the temporary isolation of affected communities. Overall, the study demonstrates that EQLs in the High Atlas are controlled by a combination of geological structure, lithology, topography, geomorphological history, and human activity, and illustrates how even moderate–magnitude events can trigger landsliding in susceptible terrain.

These findings underscore the importance of incorporating landslide hazard assessments into earthquake risk management, particularly in mountainous and infrastructure–limited regions. Understanding the spatial distribution and controlling mechanisms of



Fig. 9. Tension cracks and damage to small retaining structures along the R202/N7.

EQLs is critical for improving preparedness, guiding emergency response, and reducing future risk. In addition to the EQLs, the road infrastructure was affected by a range of geotechnical issues. Several occurrences of tension cracks, associated with cut and fill on sharp bends in the road, along the main route, were identified, together with damage to multiple small retaining structures, including failures

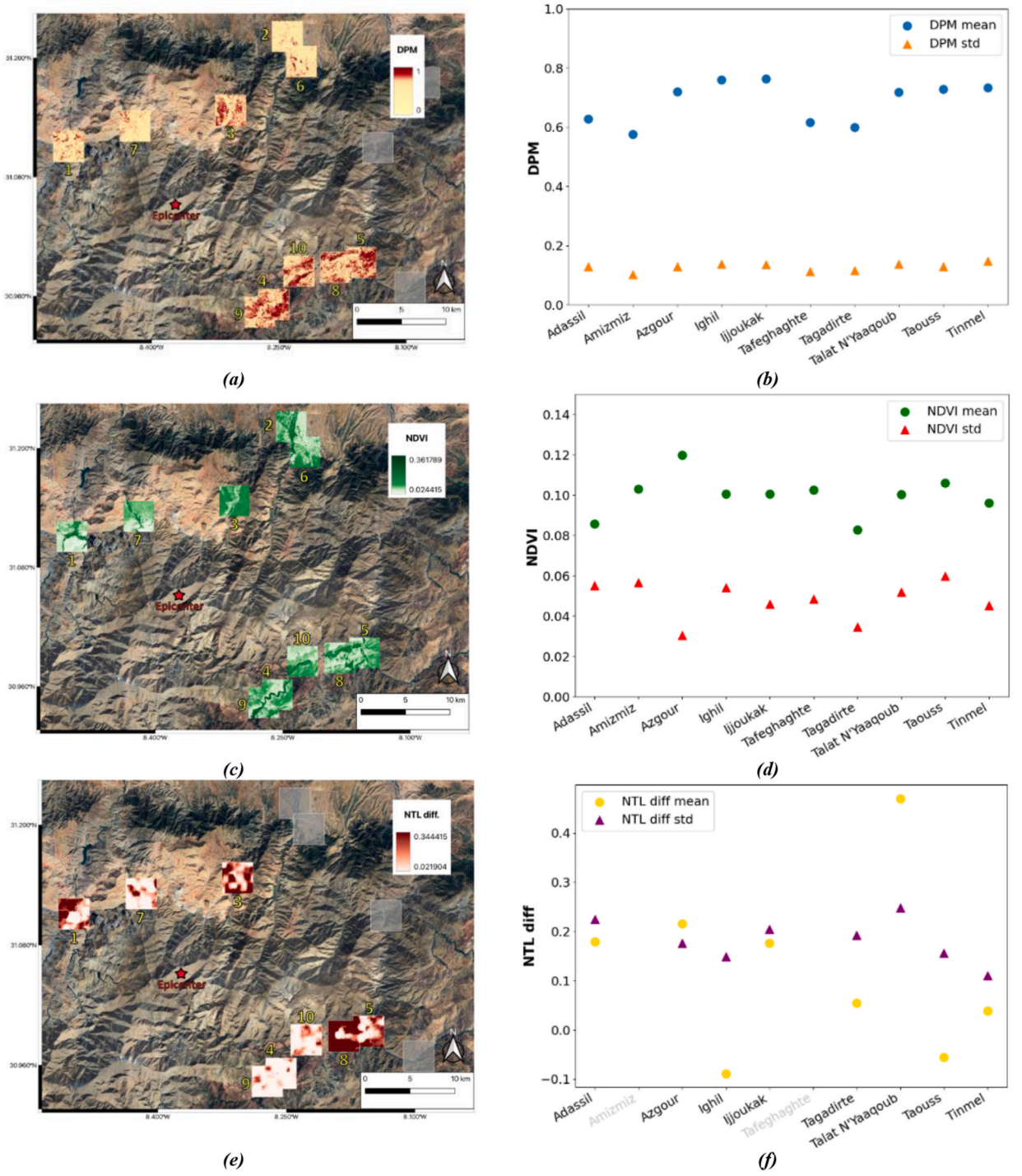

Fig. 10. Spatial distribution and statistical summaries across the High Atlas region: (a) Damage Proxy Map (DPM) values from SAR coherence change detection; (b) mean and standard deviation of DPM values across the analysed settlements; (c) Normalised Difference Vegetation Index (NDVI) values; (d) mean and standard deviation of NDVI values across the analysed settlements; (e) nighttime light (NTL) intensity changes across selected areas; (f) mean and standard deviation of NTL changes. For (b), (d), and (f), the x-axis shows the site names, ordered according to the numbering used in the maps (*e.g.*, site 1 corresponds to Adassil and appears first on the x-axis).

caused by landslide and rockfall impacts (Fig. 9).

The combined spatial analysis demonstrates that road disruption was governed primarily by the location of landslides rather than by their overall number. The spatial correspondence between the mapped EQL inventory and the principal mountain transport corridors shows that many High Atlas settlements rely on a limited number of valley roads. Consequently, relatively localised slope failures were sufficient to restrict access to remote communities, delaying rescue operations, the distribution of humanitarian assistance, and post-earthquake engineering assessments, while also influencing the prioritisation and logistics of the field reconnaissance. Field observations confirmed road blockages, failures of engineered slopes, and repeated clearance operations along the main mountain routes, providing field evidence that explained the regional accessibility patterns identified from the RS analysis.

5. Building damage and performance: observations and structural assessment

5.1. Spatial analysis of building damage (Pre–Field)

Building on the RS–based screening, a spatial framework was developed to contextualise earthquake impacts across the affected region. Administrative boundaries for the provinces of Al Haouz, Chichaoua, and Taroudant were sourced from the GADM database via the UC Davis Geodata repository [60]. These vector datasets established the basis for analysing rural municipalities (communes), including Adassil, Amizmiz, Azgour, Ighil, and Talat N'Yaaqoub. Within these communes, the analysis focused on specific settlements and villages (douars), such as Ijoukak, Tafeghaghte, Tagharte, Taouss, and Timmel. Baseline settlement data were derived from the German Aerospace Center's (DLR) World Settlement Footprint (WSF) suite [61,62]. Specifically, the WSF Evolution (WSF-EVO) dataset was used to track settlement extent at 30 m resolution for the period 1985–2015, while the WSF 3D dataset provided morphological data, such as average building height and volume, at 90 m resolution. Together, these layers enabled the generation of district-level overview maps detailing building density, footprint, height, and approximate construction age. For each analysed settlement, mean values and standard deviations were calculated from all raster pixels contained within the corresponding settlement boundary to enable consistent comparison of the DPM, NDVI, and NTL datasets across the study area.

Potentially affected areas were identified using SAR-based DPMs derived from multi-temporal coherence change detection [40,63]. This approach detects surface and structural changes by comparing interferometric coherence between pre- and post-event SAR acquisitions, where reductions in coherence indicate changes in scattering properties associated with damage [61,64–68]. DPM products used in this study were sourced from NASA's Jet Propulsion Laboratory (JPL) ARIA (utilising JAXA's ALOS–2 PALSAR–2 data [63]) and from the Earth Observatory of Singapore [69,70]. Additional DPM maps, based on Copernicus Sentinel–1 C–band imagery, were analysed to support a regional-scale assessment. An independent dataset was also generated using Sentinel-1 data processed with GAMMA SAR software [71] and the PyGMTSAR Python library [72]. The resulting DPM maps (Fig. 10a) highlight areas of strong decorrelation, which served as primary indicators for prioritising field survey locations. No absolute DPM threshold was adopted to classify earthquake damage. Instead, DPM values were interpreted comparatively, together with the complementary RS products, to identify settlements exhibiting consistently stronger disturbance signals for subsequent field reconnaissance. Statistical analysis (Fig. 10b) reveals higher mean DPM values in settlements such as Azgour, Ijoukak, Talat N'Yaaqoub, and Tinmel, reflecting significant earthquake-induced structural changes. Conversely, lower values in Amizmiz indicate comparatively limited surface disturbance. The standard deviation across all locations remained consistent, suggesting that the mean values are representative of the overall distribution and not skewed by outliers. Together, these spatial patterns provided a first-order regional screening of earthquake impacts that informed and prioritised the subsequent field reconnaissance.

Optical imagery from Landsat–8/9 [73] was used to compute the NDVI to assess whether vegetation variability influenced the SAR-based DPM signals. NDVI was computed using the near–infrared (Band 5) and red (Band 4) bands of the Landsat–8 OLI sensor. Because vegetation can cause SAR decorrelation unrelated to earthquake damage, understanding vegetation density is critical for validating coherence-based results. Landsat data are freely available and were accessed for this study through the USGS Earth Explorer portal [71]. The resulting NDVI maps (Fig. 10e) and statistical analysis (Fig. 10f) reveal generally low vegetation cover across all study sites, with mean values ranging between 0.08 and 0.12. These results are consistent with the sparse vegetation typical of the High Atlas environment. Given that Sentinel-1 C-band coherence is largely unaffected by vegetation when NDVI is below ~0.15 [72], these values suggest that vegetation did not significantly skew the DPM signals. Consequently, the observed coherence loss can be more confidently attributed to earthquake-induced disturbances caused by building damage rather than to seasonal phenological changes.

Finally, to complement the SAR-based assessment, variations in NTL intensity derived from NASA's Black Marble VNP46A2 dataset [74,75] were analysed to identify potential disruptions to electricity supply and nighttime activity. Data accessed via the Google Earth Engine (GEE) platform were filtered within a 30-day pre- and post-event window to minimise cloud contamination and ensure comparable lunar illumination. Given the coarse spatial resolution (500 m), a downscaling approach integrating Landsat-8 built-up features was applied to generate a 30 m resolution "Black Marble HD" product [76]. The resulting NTL difference maps (Fig. 10c), calculated as pre-event minus post-event intensity, highlight spatial variations across the study area. Larger decreases in NTL intensity, observed in Azgour and Talat N'Yaaqoub, indicate significant disruptions, whereas smaller changes in Ighil and Taouss suggest more limited impact. These trends are consistent with the statistical analysis shown in Fig. 10d and were used to further prioritise survey locations.

The integrated use of SAR-based damage indicators, NDVI filtering and NTL analysis provided a robust regional-scale screening of earthquake impacts. This approach facilitated the prioritisation of settlements for field reconnaissance, ensuring the survey targeted areas of high disturbance while maintaining a representative sample across varying damage severities. The field observations presented in Section 5.2–5.3.1 build upon this preliminary assessment, providing detailed insights into specific building performance and

structural failure mechanisms.

The interpretation of the RS products should be considered in the context of the inherent limitations of the individual datasets. SAR-based DPM provide regional-scale indicators of surface and structural change but may be less sensitive to localised damage in sparsely distributed rural settlements, where heterogeneous building materials, irregular settlement layouts, steep topography, and complex

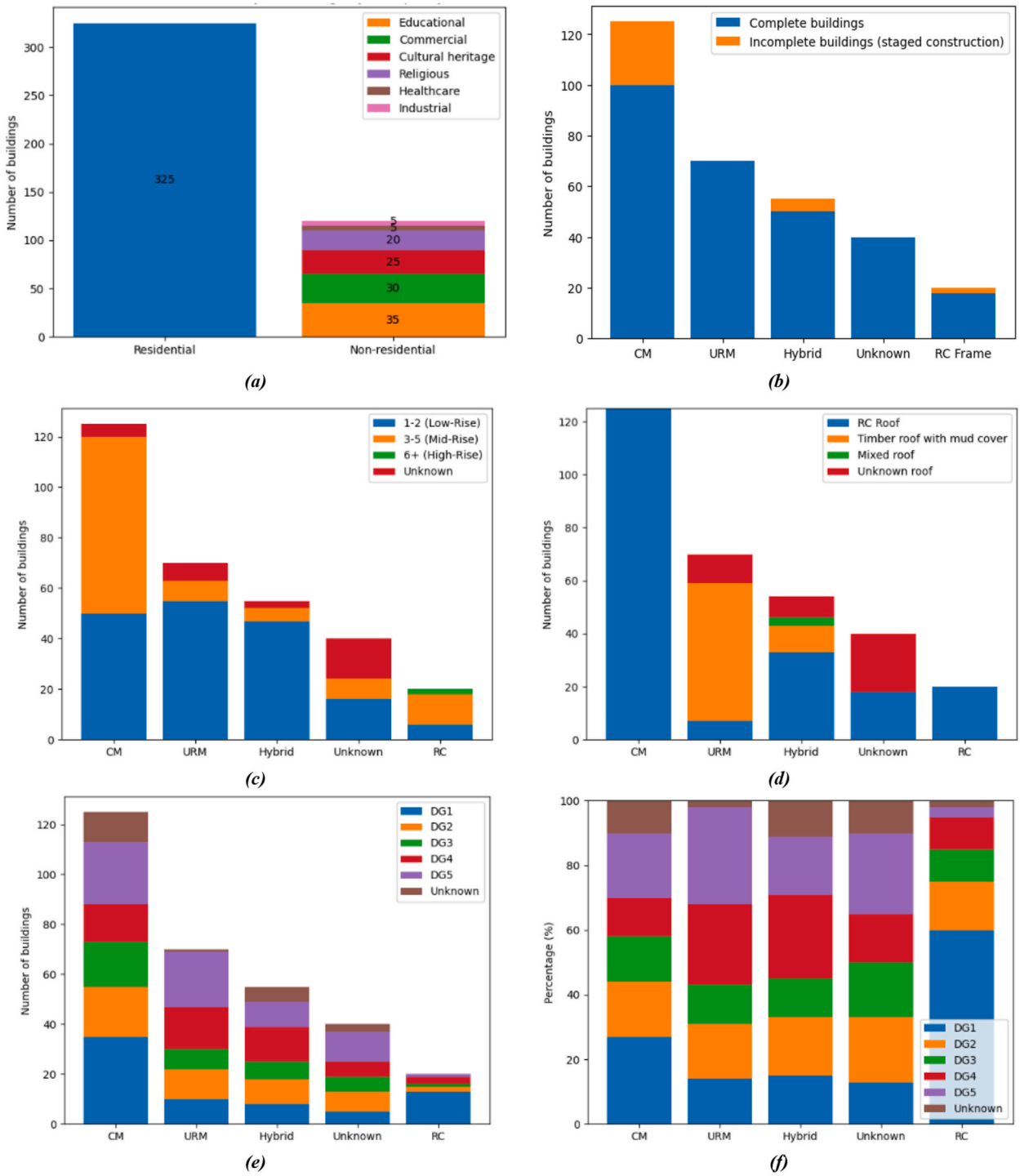

Fig. 11. Distribution of the surveyed building stock by (a) occupancy. Distribution of the surveyed residential buildings by (b) structural typologies and construction condition, (c) number of storeys, and (d) roof systems. EMS–98 damage distribution across the surveyed residential structural typologies, expressed as (e) number of buildings and (f) percentages.

radar scattering conditions can influence the coherence signal. Likewise, although the high-resolution optical imagery enabled systematic mapping of landslides, smaller failures, shallow rockfalls, or features obscured by vegetation or topographic shadow may not be fully captured. For these reasons, the RS products were not interpreted in isolation but were used as complementary indicators to guide and prioritise the field reconnaissance. The subsequent georeferenced field investigations provided the detailed engineering evidence required to refine, interpret, and contextualise the regional-scale RS observations within the combined multi-layer geospatial framework.

Based on the pre-field RS assessment described in Section 2.1, Azgour, Talat N'Yaaqoub and Ijoukak were selected as the principal survey locations because they exhibited elevated SAR Damage Proxy Map (DPM) values and significant reductions in Nighttime Light (NTL), indicating extensive structural damage. Amizmiz was selected as the principal location for the systematic building survey because its accessibility, relatively large building stock, and recommendations from local stakeholders enabled a comprehensive assessment of a broad range of building typologies and damage states. Although it exhibited comparatively lower DPM values than the priority locations, its reported damage characteristics provided an opportunity to investigate structural behaviour and damage mechanisms beyond areas characterised by widespread collapse. To complement these principal survey locations, Ouirgane was included to broaden the spatial coverage of the reconnaissance and capture a wider range of geological settings and damage conditions. Smaller settlements, including Amghrasa, Outagheri, and Tiniskt, were also surveyed because they were in areas affected by EQLs and contrasting geological and topographic conditions, providing an opportunity to investigate the influence of terrain and local site conditions on damage distribution and earthquake performance.

This combination of survey locations enabled the field campaign to document earthquake impacts across a broad range of damage severities, construction typologies, and geological settings, providing the basis for the building performance observations presented in the following sections.

5.2. Field observations and building

A total of 455 buildings were assessed across 21 urban and rural areas. The largest number of buildings was surveyed in Amizmiz (229), followed by Talat N'Yaaqoub (45), Ijoukak (41), Ouirgane (37), Azgour (18), and Amghras (14). Smaller numbers of buildings were documented in additional remote locations to broaden the geographical coverage of the survey and to investigate areas where EQLs had contributed directly to building damage or whether their principal impacts were associated with road access disruption and the temporary isolation of mountain communities. Within each location, contiguous clusters of buildings were selected for systematic survey, with all visible buildings within each cluster assessed wherever possible (Section 2.2). Fig. 11a summarises the distribution of surveyed buildings by occupancy.

Residential buildings accounted for 74% of the dataset, reflecting the dominant exposure of housing in the High Atlas region; their seismic performance is discussed in Section 5.3. Non–residential buildings, primarily religious, educational and commercial structures, are discussed in Section 5.3.1, while monumental heritage assets are examined in Section 6. Assessments relied primarily on external visual inspections, as access to buildings, particularly healthcare facilities and private dwellings, was generally restricted.

5.3. Residential buildings

Within the surveyed residential stock (Fig. 11b), confined masonry (CM) was the predominant structural typology (41.0%), followed by unreinforced masonry (URM, 22.3%). Hybrid configurations accounted for 17.1% of buildings, referring to buildings combining different structural systems or materials, most commonly URM buildings at lower storeys with CM added at upper levels. Reinforced concrete (RC) buildings only accounted for 6.1%. Approximately 12% of the surveyed structures were classified as incomplete buildings (staged construction), referring to partially built structures (*e.g.,* wall panels constructed but lacking complete floor systems). In many of these cases, construction occurred in stages over time, reflecting incremental and informal construction practices and often resulting in the combination of different structural systems or materials within the same building; these are therefore classified as hybrid configurations, as detailed in Section 5.3.3. This should be distinguished from buildings with protruding reinforcing bars (jetting rebars), which are commonly observed and typically indicate provision for future vertical expansion. Such cases are not included here, as buildings are classified based on their as-built structural typology. The year of construction and compliance with seismic design standards could not be systematically established, as many buildings had undergone incremental construction and successive modifications. Consequently, the classification is based on observed as-built structural characteristics rather than building age or presumed code compliance. A further 13.5% were classified as “Unknown”, as the structural system could not be confidently identified from the accessible field evidence owing to limited visual access and the absence of distinguishing structural features.

Approximately 60% of the surveyed residential building stock was low–rise (*i.e.,* 1–2 storey), consistent with the rural and mountainous context (Fig. 11c). Mid–rise (*i.e.,* 3–5 storey) buildings accounted for ≈30%, while high–rise (*i.e.,* 6+ storey) structures were rare. RC roof slabs were common in CM and RC buildings (≈67%), whereas timber–mud roofs remained prevalent in URM constructions (≈16%) (Fig. 11d). Fig. 11e and f presents the distribution of damage grades assessed using the EMS–98 [48], from DG1 (slight damage) to DG5 (total collapse), expressed both as the number of buildings and as relative percentages. Marked differences in seismic performance were observed among residential typologies. Excluding the buildings classified as “Unknown”, CM generally performed better, with 58% of buildings classified within DG1–DG3, although ≈20% still experienced DG4–DG5. In contrast, URM and hybrid constructions were significantly more vulnerable, with around 62% and 42% of buildings, respectively, falling within DG4–DG5. RC buildings exhibited comparatively lower damage, with ≈68% remaining in DG1–DG3 and no observed collapse.

Nevertheless, Fig. 11e and f also demonstrates that all principal structural typologies exhibited a broad distribution of EMS–98 damage grades rather than a single characteristic level of performance. Buildings of the same structural system frequently experienced markedly different damage levels. This demonstrates that structural typology alone cannot explain the observed seismic performance and highlights the importance of construction quality, structural detailing, continuity of the load path, maintenance, and local site conditions in controlling earthquake damage.

Fig. 12 presents the residential building layer, illustrating the spatial distribution of the surveyed buildings and their corresponding EMS–98 damage grades. Each georeferenced building is linked within the common geospatial framework to additional engineering attributes, including structural typology, construction materials, number of storeys, roof system, observed damage mechanisms, vulnerability characteristics, and photographic documentation (Section 2.2). This allows the spatial distribution of residential damage to be interpreted alongside complementary information on regional earthquake impacts, landslides, accessibility, geological conditions, and ground motion estimates. In Amizmiz, which represents the largest portion of the dataset, 65% of buildings fall within DG1–DG3, while ≈33% reach DG4–DG5, consistent with the comparatively lower levels of disturbance identified by the complementary RS indicators. The systematically surveyed buildings in this area were relatively diverse, comprising ≈50% CM, ≈13% RC frame structures, and ≈12% traditional URM buildings, with the remainder corresponding to hybrid or unknown structural types. In contrast, Ijoukak and Talat N'Yaaqoub exhibited substantially higher damage levels, with ≈50% and ≈54% of buildings, respectively, reaching DG4-DG5, in agreement with the higher levels of disruption identified through RS indicators. In Ijoukak, the building stock consisted of URM construction (≈23%), CM structures (≈20%) and hybrid systems (≈14%) with the remainder corresponding to unknown structural types, while RC frame buildings were rare. In Talat N'Yaaqoub, the corresponding percentages for URM, CM, and hybrid buildings were 22%, 24%, and 29%, respectively. Ouirgane, which was not identified as one of the principal priority areas during the pre-field RS assessment, presented an intermediate pattern, with ≈39% of buildings falling within DG4–DG5 and a hybrid building stock composed mainly of URM (≈52%), RC (≈21%), CM (≈15%), with the remainder corresponding to hybrid and unknown structural types.

As illustrated in Fig. 12, the spatial distribution of the surveyed building damage is broadly consistent with the regional ShakeMap-derived PGA contours. However, these estimates should be interpreted as providing regional context rather than precise representations of local ground motion. Consequently, the observed spatial variability in building damage should not be interpreted as resulting from estimated PGA values alone. Instead, the common geospatial framework enables regional-scale ground motion estimates to be interpreted alongside detailed georeferenced building observations, EQL mapping, road access disruption, geological and topographic information, and engineering assessments, providing the broader environmental and structural context needed to interpret the observed variability in earthquake impacts.

To further interpret these patterns, Table 1 synthesises the quantitative damage distributions presented in Fig. 11e and f and Fig. 12 together with the principal vulnerability characteristics and dominant failure mechanisms identified during the onsite field reconnaissance for each residential structural typology. The table links structural typology with EMS–98 damage distribution, observed vulnerability characteristics, and dominant failure mechanisms, while the engineering evidence underpinning these observations is presented and discussed in detail in Sections 5.3.1–5.3.4. Representative examples illustrating this variability are also presented in Sections 5.3.1–5.3.4, where buildings of the same structural typology are shown to exhibit markedly different seismic performance owing to differences in construction quality, detailing, maintenance, structural irregularities, and local site conditions.

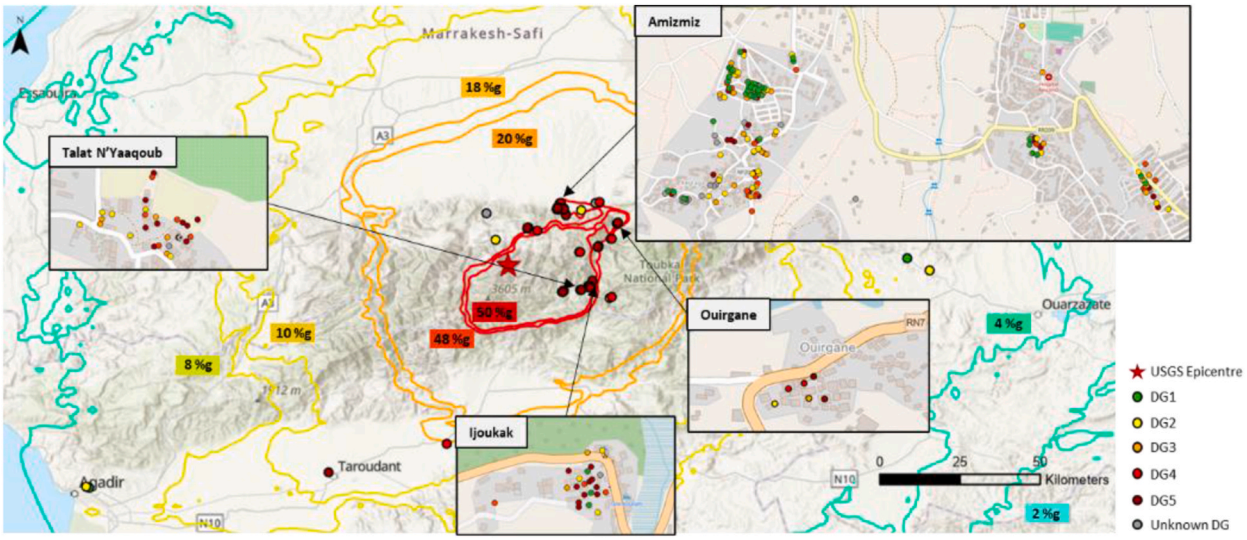

Fig. 12. Residential building layer, showing the spatial distribution of the surveyed residential buildings and their corresponding EMS–98 damage grades. The figure also includes the USGS ShakeMap-derived peak ground acceleration (PGA) contours (%g) and the location of the 8 September 2023 Mw 6.8 Al Haouz earthquake epicentre [1].

Table 1
Synthesis of the field reconnaissance, linking observed EMS–98 damage distributions with principal vulnerability characteristics and dominant failure mechanisms for the main residential structural typologies.

Structural typology	Observed EMS–98 damage distribution	Principal vulnerability characteristics	Most frequent observed failure mechanisms
Confined masonry (CM)	Predominantly DG1–DG3, with approximately 20% classified as DG4–DG5	Poor reinforcement detailing, inadequate confinement, lack of toothing between masonry and RC tie-elements, poor-quality masonry units and mortar, plan and vertical irregularities	Diagonal shear cracking (~50%); overturning of masonry wall panels (~50%); crushing and spalling of masonry (~30%); partial roof collapse (~20–25%)
Unreinforced masonry (URM)	Predominantly DG4–DG5, with approximately 62% classified as DG4–DG5	Weak mortar and material cohesion, poor wall-to-roof and corner connections, lack of transverse ties, heavy roofs, flexible timber diaphragms, poor maintenance, irregular configurations and buildings founded on slopes	Out-of-plane wall failures (~55%); corner failures (~30%); roof collapse (~30%); in-plane shear cracking (~20%); pounding-induced damage (~10%)
Hybrid construction	Predominantly DG3–DG5, with approximately 42% classified as DG4–DG5	Incremental (staged) construction, different structural systems between storeys, weak connections, structural irregularities (vertical irregularity, setbacks, irregular plans), discontinuous load paths and incompatible materials	Differential structural response between construction phases, interface cracking/ failures (≈40%), partial collapse of added upper storeys and roofs (≈30%), local wall collapse, diagonal shear cracking
Reinforced concrete (RC) frame with masonry infill	Predominantly DG1–DG3, with approximately 68% classified as DG1–DG3 and no observed collapse	Plan and vertical irregularities (balconies, setbacks, re-entrant corners, transferred structures), soft-storey configurations, short columns, inadequate detailing, poor infill-frame interaction, irregular configurations	Infill wall cracking (diagonal and around openings) (~45–50%); plaster spalling/local crushing (~30%); local panel dislodgement (~20%); soft-storey mechanisms (~10%); pounding-induced damage (~10–15%)

Note: The EMS–98 damage distributions were derived from the complete onsite survey*, while the percentages reported for the dominant failure mechanisms were calculated from the onsite field reconnaissance dataset and represent the proportion of surveyed buildings within each structural typology exhibiting the corresponding mechanism.* Individual buildings frequently exhibited more than one failure mechanism; therefore, the reported percentages are not mutually exclusive and do not sum to 100%.

5.3.1. Confined masonry buildings (CM)

In the Moroccan seismic code (RPS 2000), CM is referred to as Maçonnerie Chaînée (literally "chained masonry") and is addressed within the masonry building requirements, particularly Article 7.3.3.2 (Construction and detailing of masonry walls) [47]. However, unlike internationally recognised CM standards [77–80], the RPS does not define CM as a distinct structural system with dedicated seismic design procedures. Instead, the provisions focus primarily on construction detailing and the inclusion of RC tie-elements within masonry construction, without explicitly defining the structural role of the masonry walls and RC confining elements or identifying the walls-first construction sequence as a defining characteristic of the CM system [81]. Consequently, buildings incorporating both masonry and RC elements are frequently described locally as Maçonnerie Chaînée, irrespective of whether the masonry walls function as the primary gravity- and lateral-load-resisting system or as non-structural infill within an RC frame.

This creates ambiguity, as the structural system cannot be determined reliably from the locally adopted terminology alone. Consequently, reliable classification requires engineering interpretation of the structural configuration and the respective roles of the masonry walls and RC elements. Accordingly, buildings were classified as CM when the masonry walls constituted the principal gravity- and lateral-load-resisting system, while the RC tie-columns and tie-beams provided confinement without forming an independent structural frame, such that the masonry walls and RC confining elements acted compositely as an integrated structural system. Construction deficiencies, including poor detailing or inadequate confinement, were not considered sufficient to alter this classification. These buildings were therefore considered deficient examples of CM rather than a different structural typology. Buildings in

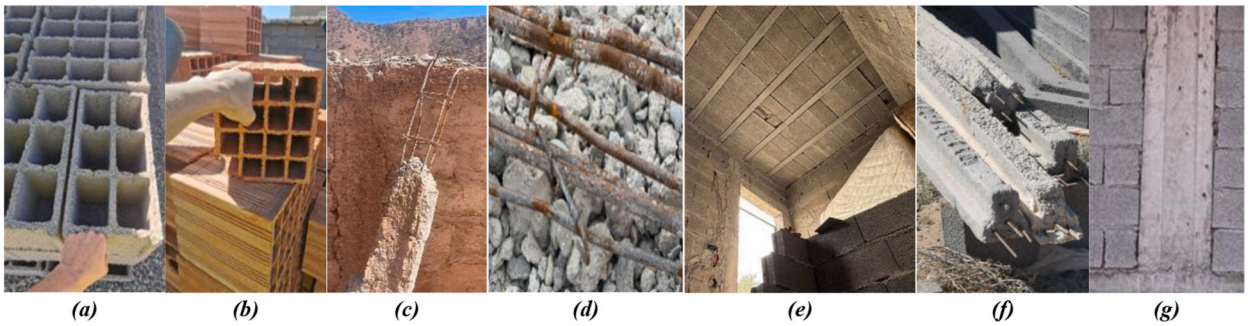

Fig. 13. (a) Concrete Masonry Units (CMUs) with large voids and insufficient web thickness; (b) hollow clay bricks with large voids and insufficient web thickness; (c) poor reinforcement in the Reinforced Concrete (RC) tie–elements (d) debris showing poor–quality concrete and smooth reinforcement bars used for the RC elements; (e) Confined Masonry (CM) panels and floor system composed of RC joists and CMU infills; (f) typical RC joists used in CM floor construction; (g) lack of toothing between masonry walls and RC tie–columns.

which the RC members formed a continuous structural frame resisting the majority of the gravity and lateral loads were classified as RC frame buildings with standard masonry (*e.g.* clay or concrete masonry units (CMUs)) infill (Section 5.3.4). Buildings exhibiting characteristics of both systems, typically associated with staged or incremental construction were classified as hybrid frame-wall systems (Section 5.3.3). This category included buildings in which RC framing was combined with traditional masonry materials (*e.g.*, rammed earth (RE) or stone masonry (SM)), resulting in structural configurations that did not conform to either conventional CM or typical RC frame buildings with masonry infill. Where the available field evidence was insufficient to distinguish confidently between these structural typologies, the buildings were classified as Unknown.

Based on these criteria, buildings classified as CM appear to be widely distributed across both rural and urban areas of Morocco and include both single- and multi-storey construction. However, this observation cannot be verified using the available census data [46], as the reported building categories do not distinguish between different masonry structural systems, reflecting the absence of a dedicated structural classification for CM within the Moroccan seismic code. Approximately 70% of the surveyed CM buildings were constructed using CMUs, while approximately 25% were constructed using hollow clay bricks with large voids and thin webs (Fig. 13a and b). Although all of these buildings satisfied the adopted classification criteria for CM, they exhibited substantial differences in construction quality and detailing. Common deficiencies included inadequate dimensions and detailing of the RC confining elements, insufficient anchorage, smooth reinforcement bars, and poor-quality concrete (Fig. 13c and d). Masonry wall panels frequently exhibited damaged or poorly manufactured units, irregular mortar joints and weak mortar (Fig. 13e), while the floor systems typically comprised RC joists with CMU infill blocks that also exhibited inadequate reinforcement detailing (Fig. 13e and f). A lack of proper toothing between the masonry walls and RC tie-columns was also frequently observed (Fig. 13g), limiting the mechanical interlock and reducing the composite action between the masonry walls and the RC confining elements.

The construction deficiencies illustrated in Fig. 13 are reflected in the observed damage patterns. Fig. 14 presents the principal in-plane failure mechanisms identified in the surveyed CM buildings. Shear-related damage, characterised by diagonal or X-shaped cracking across masonry wall panels, was observed in approximately 50% of the surveyed buildings, predominantly around corners and openings where stress concentrations developed. Localised crushing and spalling within compression zones were identified in approximately 30% of the buildings, particularly adjacent to RC tie-columns and wall edges and were generally associated with the most severe damage states. These damage mechanisms were frequently accompanied by poor masonry quality (Fig. 14a–c) and were further exacerbated by structural irregularities. Buildings exhibiting vertical irregularities, typically associated with a reduced upper-storey height relative to the ground floor, commonly developed cracking that initiated at the second storey. Similarly, buildings with plan irregularities, particularly jetty-type configurations, exhibited torsional effects that contributed to increased damage concentrations (Fig. 14d and e).

Out-of-plane instability and roof collapse represented the most severe damage states observed within the CM building stock (Fig. 15). Complete roof failure occurred in approximately 20-25% of the surveyed buildings and was predominantly initiated by overturning of masonry wall panels, representing the dominant collapse mechanism (approximately 50% of cases; Fig. 15a and b). Wall overturning frequently triggered progressive collapse involving beam-wall and column-wall interfaces (Fig. 15c). Damage at beam-wall and column-wall interfaces was identified in approximately 5% and 10% of the surveyed buildings, respectively. Similar interface failures were also observed in buildings that did not experience complete roof collapse (Fig. 15d), where panel dislodgement, severe material degradation and exposed reinforcement indicated poor concrete quality, inadequate confinement and deficient reinforcement detailing.

The damage mechanisms described above are representative of buildings that satisfied the adopted classification criteria for CM. However, because buildings incorporating RC elements within traditional masonry construction are commonly referred to locally as *Maçonnerie Chaînée*, field reconnaissance identified a small number of buildings whose structural classification required further engineering interpretation. Representative examples are presented in Fig. 16 because they illustrate the ambiguity associated with the locally adopted terminology and the practical application of the adopted classification methodology. The discussion below focuses on the structural characteristics that led to their exclusion from the CM category, while a detailed description of this structural typology is provided in Section 5.3.3.

In the buildings shown in Fig. 16a and b, the RE and SM walls may have been constructed before the RC tie-elements were cast.



Fig. 14. Confined Masonry (CM) buildings showing (a–c) X-shaped and diagonal shear cracks, with localised crushing and spalling of Concrete Masonry Units (CMUs) associated with poor masonry quality; (d) vertical irregularity; and (e) plan irregularity.



Fig. 15. Confined Masonry (CM) buildings showing roof failure driven by: (a–b) overturning of panels; and failures at beam–wall (c) and column–wall interfaces. CM building showing (d) panel dislodgement and material loss in columns with exposed reinforcement.

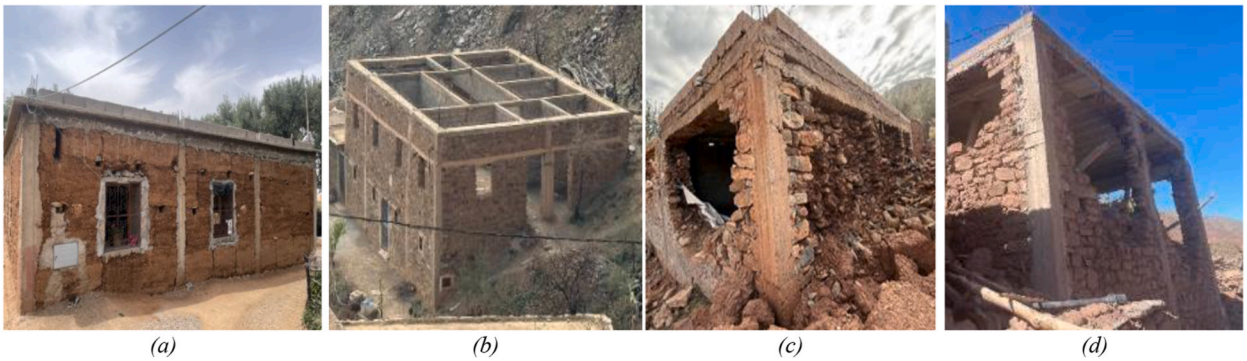

Fig. 16. (a) Hybrid frame-wall system comprising RC framing combined with rammed earth (RE); (b) hybrid frame-wall system comprising RC framing combined with stone masonry (SM); (c–d) hybrid frame-wall system comprising RC framing with stone masonry (SM) wall panels exhibiting characteristic arch-shaped cracking.

However, the absence of effective mechanical interlocking between the masonry walls and the RC elements (Fig. 16a), together with the excessive spacing of the RC tie-elements (Fig. 16b), prevented the development of the composite action that characterises conventional CM. Consequently, these buildings did not satisfy the adopted CM classification criteria and were excluded from the CM category.

By contrast, the buildings shown in Fig. 16c and d exhibit relatively large RC members forming a continuous structural framework around the SM walls. Although the original construction sequence cannot be established from post-earthquake reconnaissance alone, the observed structural configuration and damage patterns indicate that the masonry walls and RC elements did not develop the composite action expected in conventional CM. Furthermore, the thick traditional stone masonry walls cannot be assumed to function solely as non-structural infill, distinguishing these buildings from conventional RC frame buildings with masonry infill. This interpretation is supported by the extensive damage observed within the stone masonry, including arch-shaped cracking, dislodgement of masonry units and, in multi-leaf SM, separation of the external leaf (Section 5.3.2). These damage mechanisms are consistent with frame–wall interaction rather than the integrated behaviour expected in conventional CM. Consequently, these buildings did not



Fig. 17. URM typologies (a) RE; and (b) SM. Construction details: (c) RE with gravels and small pebbles; (d) RE with straw; (e) rounded SM; and (f) flat SM.

satisfy the defining characteristics of either conventional CM or conventional RC frame buildings with masonry infill and were therefore excluded from the CM category. Their classification as hybrid frame-wall systems is discussed in Section 5.3.3.

5.3.2. *Unreinforced masonry buildings (URM)*

URM typologies (Fig. 17a and b) represent the predominant traditional building stock in the surveyed settlements and exhibited the highest proportion of severe damage within the EEFIT dataset (Fig. 11c and d). The most severe damage occurred in villages located near the epicentre (Fig. 1), where strong ground shaking intensity and possible local site amplification effects were reported [82–85]. The following section first describes the material and construction characteristics of URM typologies, including wall and roof systems, and then links these to the global seismic failure mechanisms observed in the field.

Within the surveyed URM buildings, 57% were constructed using load bearing RE walls, compacted in situ within formwork and typically incorporating gravel, small pebbles, and straw (Fig. 17c and d). These structures are built on elevated stone plinths to mitigate the impact of ground water and rising damp [18–25]. RE construction relies on layered compaction within formwork, making material quality and interlayer bonding critical to structural integrity [86,87]. Evidence of poor compaction and weak cohesion in RE buildings was observed, leading to vertical cracking along construction joints in approximately 20% of cases (Fig. 17a). Partial abandonment and irregular maintenance further exacerbated material degradation.

The remaining URM stock consisted of load-bearing SM walls constructed with irregular, rounded, or flat granite or limestone stones (Fig. 17e and f). SM buildings were historically associated with more affluent households due to higher construction costs compared to RE [88–90]. SM walls typically comprise two stone leaves enclosing a cavity filled with loosely bonded rubble and low–quality mortar (Fig. 18a). Consistent with typical multi–leaf masonry behaviour under lateral loads [91–93], SM walls exhibited material loss (Fig. 18b) and leaf separation (Fig. 18c and d). These material-level damage mechanisms, when combined with roof hammering in the direction of seismic loads, often lead to out-of-plane arch-type failures at the wall crest (Fig. 18e–g), ranging from partial material loss to complete collapse.

The predominant floor system in URM buildings (≈80%) consisted of flat timber roofs, covered with compacted mud (Fig. 19a). Primary beams (Fig. 19b) often lacked full-span continuity or adequate overlap, while secondary elements consisted of small wooden branches or bamboo (Fig. 19b–d). Beams often passed through the bearing walls and extended beyond the external face but were typically seated directly on the masonry or on loose stone layers at the wall crest (Fig. 19c).

This configuration creates weak interfaces and localised stress concentrations, evidenced by vertical cracks (Fig. 20a), reducing load transfer. Perimeter timber bands tying walls together and enhancing wall–roof interaction were observed only in retrofitted URM buildings or later additions (Fig. 20b). The high flexibility of the roof diaphragm, combined with limited in–plane stiffness and poor wall–roof connections, contributed to partial or total roof collapse in ≈30% of buildings. In ≈10% of cases, the original lightweight timber roofs were replaced with heavier RC slabs, increasing seismic demand and thereby contributing to collapse (Fig. 20c).

Out-of-plane wall failures were among the most recurrent mechanisms, affecting approximately 55% of URM buildings and including the arch-type behaviour described above for SM walls. Representative examples for RE and SM are shown in Fig. 21a and 22a. In RE buildings, typically built as isolated units (*e.g.,* detached house) and therefore lacking lateral restraint from adjacent buildings, overturning susceptibility was further increased by construction sequences in which longer walls, built before shorter transverse walls, lacked adequate corner interlocking (Fig. 21b). This mechanism was characterised by vertical cracking at the wall edges. In contrast, SM buildings were noted in both isolated and clustered configurations. Isolated SM buildings (Fig. 22a and b) were significantly more vulnerable to partial or total out–of–plane collapse than clustered ones, with failures characterised by stone loss and progressive separation of the external leaf (Fig. 22c). Corner failures were also widespread (≈30%), affecting both RE and SM buildings (Fig. 21c and d and Fig. 22b, respectively). In clustered SM buildings, particularly those with plastered walls (Fig. 22c–e), increased lateral restraint limited the development of out-of-plane collapse. In these cases, out-of-plane behaviour was primarily manifested through vertical cracking without significant material loss (Fig. 22c). Consequently, in-plane failure modes (Fig. 22d) occurred in ≈20% of URM buildings. Pounding between adjacent buildings was also identified in ≈10% of cases, leading to localised damage at the contact zones (Fig. 22e).

Traditional strengthening measures reflecting local awareness of past earthquakes [84] were observed in RE buildings, including

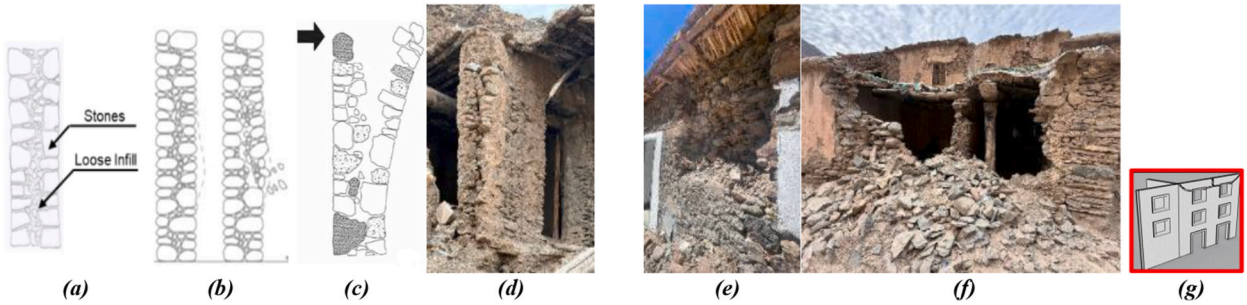

Fig. 18. (a) Schematic of a multi-leaf SM wall, modified from Ref. [91]; (b) schematic of leaf separation due to material loss, modified from Ref. [92] (c) schematic of leaf separation due to roof hammering, modified from Ref. [93]; (d) leaf separation; (e) severe and (f) complete collapse due to arch-type failure. (g) Arch failure mode sketches adapted from Ref. [94].



Fig. 19. Timber floor/roof system: (a) timber roof with compacted mud; (b) primary beams with secondary branch elements; (c) stone layer beneath the roof at the wall crest; (d) primary beams with secondary bamboo canes.

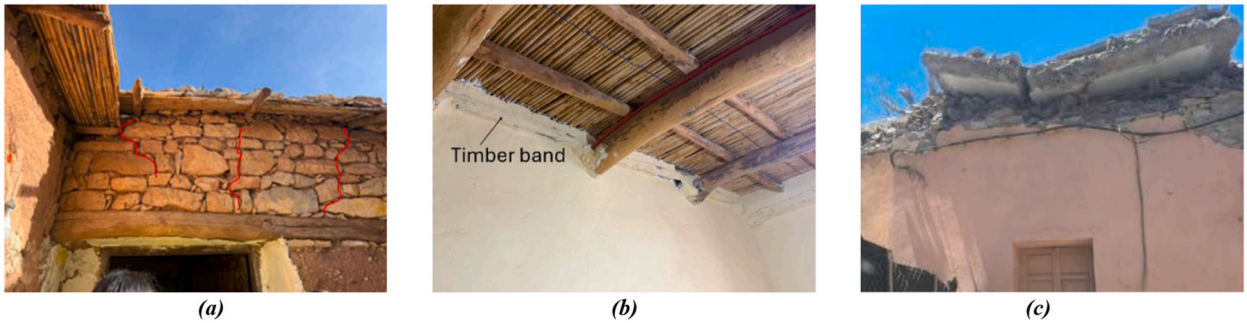

Fig. 20. (a) Vertical cracking due to reduced load transfer; (b) timber band below the roof; (c) RC slab replacing the original timber roof.

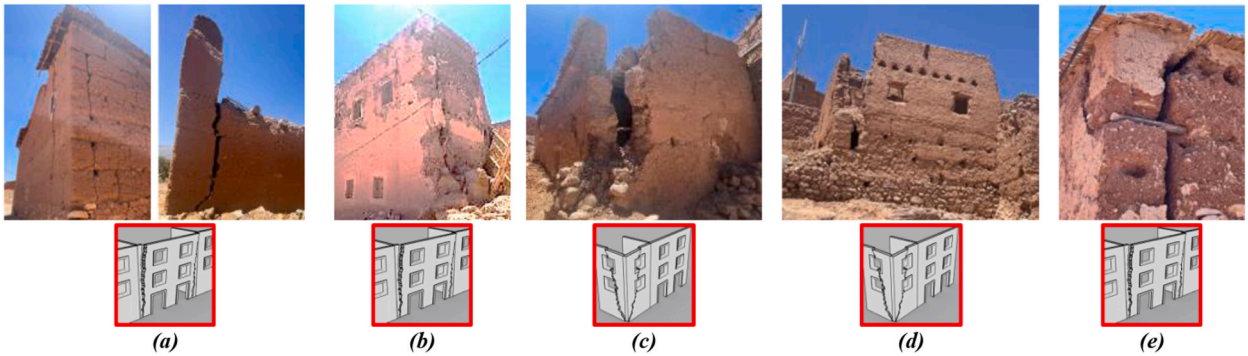

Fig. 21. RE buildings showing (a) severe vertical cracking along block joints; (b) out–of–plane failure; (c–d) corner failures; (e) smooth timber ties at the corner. Failure mode sketches adapted from Ref. [94].

timber ties inserted at wall corners to improve connections (Fig. 21e). However, their smooth surfaces and insufficient anchorage often failed to prevent wall separation and corner failures.

Similar strengthening measures were identified in SM buildings, including wooden lintels above openings (Fig. 23a), elongated cornerstones enhancing interlocking (Fig. 23b), and timber pegs connecting wall wythes and orthogonal corners (Fig. 23c). Despite generally better preservation in SM buildings, their application remained irregular and non-systematic, limiting their effectiveness in controlling crack propagation and preventing leaf separation and overturning (Fig. 23d). Buildings shown in Fig. 23a and b, where maintenance or strengthening interventions were more systematic, exhibited reduced damage. In contrast to conservation principles aimed at preserving traditional construction techniques, recent URM construction often incorporates RC elements under the assumption that modern materials inherently improve seismic performance. This practice is particularly common in SM buildings, where RC ring beams and slabs are introduced during construction (Fig. 24a). However, effective connections with the brittle masonry walls are rarely achieved, leading to dislodgement at the wall–roof interface and out–of–plane failures characterised by arch–shaped cracking (Fig. 24b), often resulting in partial or complete roof collapse (Fig. 24c and d). In several cases, these failures were more severe than those observed in traditional URM buildings without RC additions.

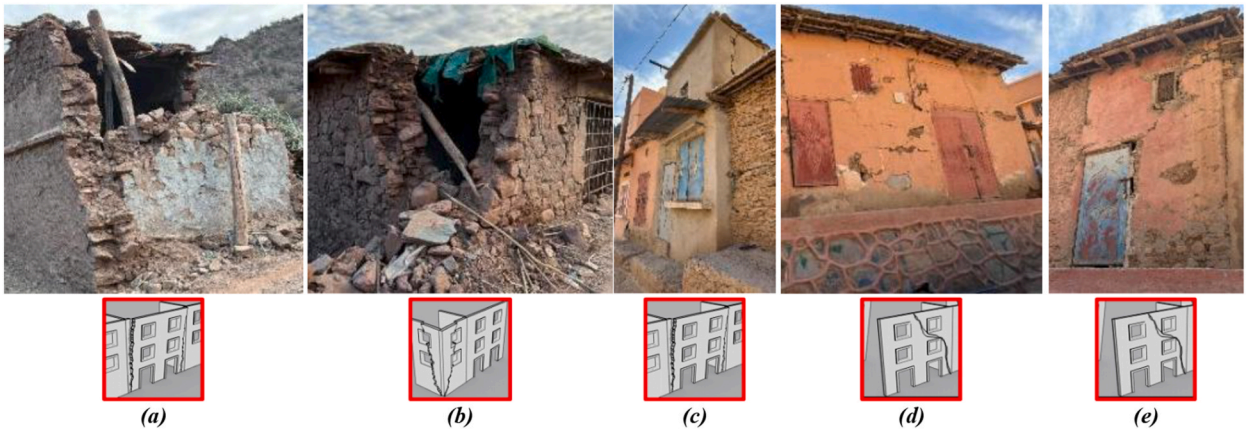

Fig. 22. SM buildings: isolated configurations with (a) out–of–plane failure and (b) corner failure; clustered configurations with (c) out–of–plane failure, (d) in–plane failure, and (e) pounding between adjacent buildings. Failure mode sketches adapted from Ref. [94].

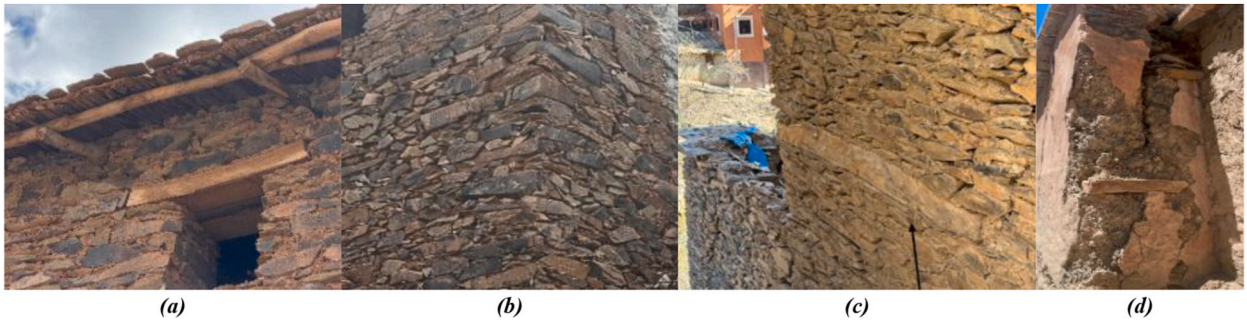

Fig. 23. (a) Timber lintels above openings; (b) cornerstones enhancing interlocking; (c) timber stitches/dowels within the wall; (d) timber dowels at corners.



Fig. 24. (a) SM building with RC beams at lintel and roof levels; (b) out–of–plane wall dislodgement from the RC beam; (c) RC roof collapse; (d) failure of a lightly reinforced RC slab.

5.3.3. Hybrid buildings

Hybrid buildings, defined by informal incremental construction practices involving staged extensions, varied structural systems, and mixed materials, typically guided by local know–how rather than formal engineering design [95–97], were commonly observed in rural villages of the High Atlas region near the epicentre (Fig. 1). EEFIT post–earthquake reconnaissance indicates that this typology exhibited poor seismic performance, accounting for a substantial proportion of severe damage states (more than 50% in DG3 or above; Fig. 11e and f). Their behaviour is interpreted within a three-stage informal construction process, which provides a structured framework to classify the main forms identified in the field. Similar processes have been documented in Kenitra, Morocco [98], consistent with patterns observed in the High Atlas. Accordingly, three principal forms are identified, corresponding to progressive stages of construction: (i) temporary shelter configurations with incomplete structural systems; (ii) intermediate housing with partially completed vertical and horizontal elements; and (iii) permanent housing characterised by completed but heterogeneous structural systems.

Stage 1—Temporary Shelter consists of a partially completed ground floor constructed with reused materials to establish an initial dwelling footprint [98]. In practice, these configurations may remain in this incomplete state for extended periods due to financial constraints. Two typical configurations corresponding to the CM typology (Section 5.3.1), are observed. The first (Fig. 25a) comprises RC tie–columns and beams with CMU wall panels, where the slab has not yet been constructed. The absence of diaphragm action leaves the walls unsupported and highly susceptible to out-of-plane failure. The second (Fig. 25b) includes RC tie–columns and beams with SM wall panels with a temporary traditional floor, with characteristics and deficiencies similar to those described in Fig. 19. As discussed in Section 5.3.1, the ineffectiveness in the confinement between RC elements and masonry infill, due to material incompatibility and incorrect construction sequence, leads to arch-type panel failure (Fig. 17) associated to masonry leaf separation (Fig. 18).

Stage 2—Intermediate Housing is characterised by the completion of a permanent floor system at least at the first level, marking the transition from a temporary shelter to a more structurally consolidated occupation. This stage often involves partial development of upper storeys as income-generating units, commonly through informal rental or *Rahn* arrangements [98]. The generated income is typically reinvested into subsequent construction phases, linking structural consolidation with incremental financing. The building shown in Fig. 25c illustrates this condition: the first storey comprises CM with SM infill panels, while the temporary floor (Fig. 19) has been replaced with an RC joist–CMU slab (Fig. 13e). At the upper storey level, only the CMU walls have been partially constructed, with an RC sill band in place, while the slab has not yet been completed. Fig. 25d provides a further example of this condition. In this case, the same structural system and materials are used. However, only the masonry panels are constructed, and no floor system is present, resulting in a cantilever behaviour of the walls. Projecting reinforcement bars, left for future extensions, further increase the risk of corrosion.

Stage 3—Permanent Housing represents the final phase in the construction (Fig. 26), where temporary elements are replaced with permanent materials and finishes, or where existing buildings are vertically extended through successive construction stages, resulting in hybrid structural behaviour driven by the interaction between existing and newly added storey or components, often characterised by incomplete interfaces, poor bonding, and unfinished elements. Nonetheless, substantial heterogeneity in construction quality persists, reflecting household financial capacity. Some buildings remain unfinished (Fig. 26a), while others exhibit partial or "patched" construction with mixed materials (Fig. 26b and c). Material and detailing heterogeneity, discontinuous load paths, and incompatible deformation capacities, combined with the deficiencies outlined in Section 5.3.1 and 5.3.2, often lead to local brittle failure mechanisms, typically concentrated at storeys where changes of the structural system occur rather than resulting in a global structural response. Observed failures include diaphragm failure due to inadequate anchorage, severe shear cracking, overturning of unanchored infill panels, and plastic hinging of columns in stiffer upper storeys, frequently culminating in localised corner failures (Fig. 26c–e). This complexity hinders the clear identification of dominant failure mechanisms and complicates decision-making regarding appropriate interventions, particularly when choosing between retrofit and replacement.

5.3.4. *Reinforced concrete buildings (RC)*

RC buildings represented only a small fraction of the structures surveyed in settlements close to the epicentre (Fig. 1). In many cases, as discussed in Section 5.3.1, distinguishing between RC moment–frame systems and CM was challenging because buildings incorporated heavy masonry infills and had RC beams and columns with relatively small cross-section. Several of these buildings experienced moderate to severe damage, including partial and localised collapses—most commonly at upper storeys, such as terrace levels (Fig. 27a). The extent of damage is mainly linked to shortcomings in construction quality, detailing, and structural irregularities, rather than to intrinsic weaknesses of the RC system. Typical damage patterns included extensive in-plane shear cracks in walls, horizontal cracking at slab levels, and diagonal cracks around openings, often accompanied by the dislodgement or complete loss of infill panels (Fig. 27b–e). Additional observations included plaster spalling and partial failure of wall and roof elements, particularly at weak wall–slab connections. Multiple vulnerability factors contributed to the observed damage. Vertical and horizontal irregularities—such as variable storey heights, irregularly distributed openings, re–entrant corners, setbacks, and overhanging volumes—were present. Other common weaknesses included soft–storey mechanisms and short–column effects. Buildings constructed on sloping terrain exhibited even more complex behaviour due to uneven load paths and torsional responses. Similar to other construction typologies, non–structural components—parapets, chimneys, and roof overhangs—proved particularly susceptible to damage, often cracking or collapsing because of weak anchorage and heavy roofing systems.



Fig. 25. Temporary shelter: (a) Confined Masonry (CM) with Concrete Masonry Units (CMU) panels without first–floor slab; (b) CM with stone masonry (SM) panels with traditional floor. Intermediate Housing: (c) CM with SM panels with a reinforced concrete (RC) sill band enclosing short CMU, (d) CM with CMU panels without the sill band.

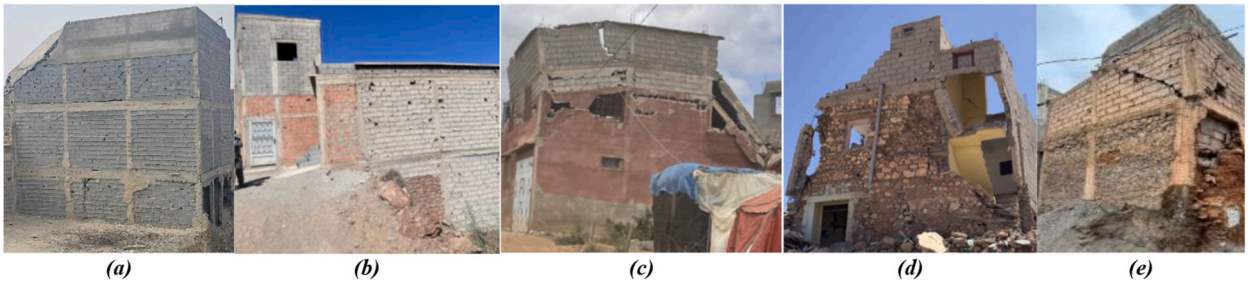

Fig. 26. Permanent housing: (a) without finishes, (b) with partial finishes, (c–e) observed failures of hybrid buildings.



Fig. 27. Reinforced concrete (RC) buildings in settlements close to the epicentre: (a) failure of upper storey; (b) shear cracking in infill walls; (c–e) dislodgement and loss of infill panels.

In contrast, RC buildings constituted the predominant construction typology in Agadir. Following the extensive destruction caused by the 1960 earthquake, reconstruction in the city incorporated modern construction techniques and seismic design provisions. Although ground shaking in Agadir during this event was significantly lower (Fig. 1), the RC building stock demonstrated markedly superior performance. Field observations revealed only limited instances of damage, and these were generally minor, affecting primarily non–structural elements such as cracking at seismic joints and slight damage to finishes (Fig. 28). This comparison underscores the positive influence of code–compliant design and sound construction practice on the seismic performance of RC buildings.

5.4. Non–residential buildings

Non-residential buildings—including mosques, schools, healthcare facilities, hotels, commercial, and industrial buildings—were also inspected during the field reconnaissance mission. Following the methodology described in Section 2.2, the georeferenced observations collected for these buildings were incorporated into the multi-layer post-earthquake framework as the non-residential building layer. Although these buildings generally follow construction practices similar to those identified for residential buildings (Section 5.3), differences in structural configuration, occupancy, code compliance, and construction quality may influence their seismic response. Fig. 29 presents the non-residential building layer, showing the spatial distribution of the surveyed buildings and their corresponding EMS–98 damage grades [48]. For clarity, only the building type and EMS–98 damage grades are displayed; however, each georeferenced building is linked within the thematic layer to the full set of engineering observations collected during the field reconnaissance (Section 2.2), including structural typology, construction materials, number of storeys, roof system, observed



Fig. 28. Reinforced concrete (RC) buildings in Agadir: (a–c) Cracking observed at seismic joints; (d) Light damage to non–structural elements.

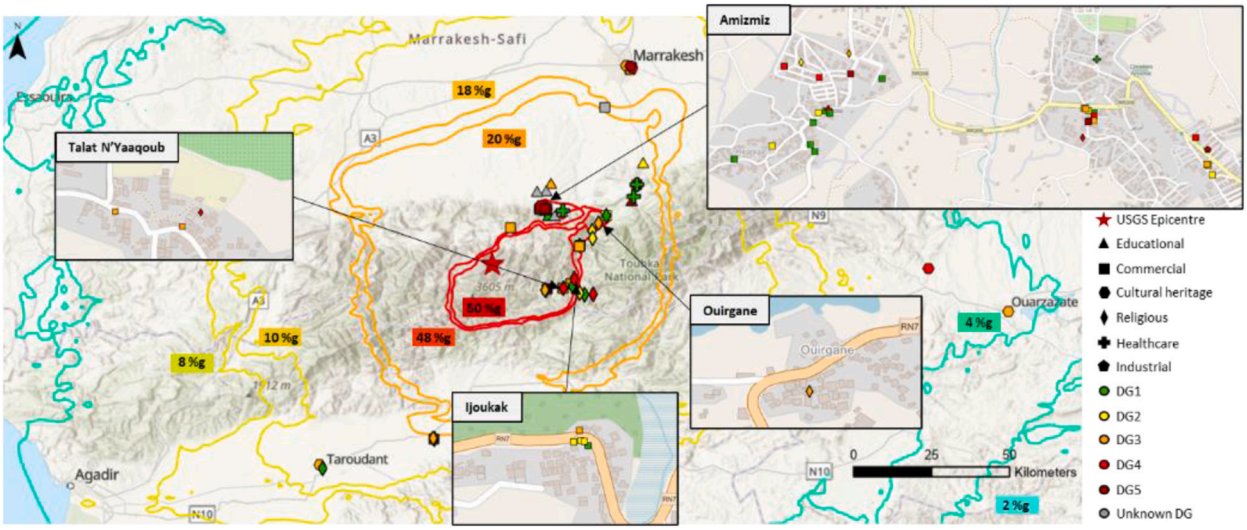

Fig. 29. Non-residential building layer, showing the spatial distribution of the surveyed non-residential buildings—including religious (mosques), educational (schools), healthcare, commercial, industrial buildings and designated cultural heritage buildings —and their corresponding EMS–98 damage grades. The figure also includes the USGS ShakeMap-derived peak ground acceleration (PGA) contours (%g) and the location of the 8 September 2023 Mw 6.8 Al Haouz earthquake epicentre [1].

damage mechanisms, vulnerability characteristics, photographic documentation, and other survey attributes. As with the residential building layer, the observed damage patterns are interpreted within the common geospatial framework rather than in isolation, allowing non-residential building performance to be evaluated alongside the regional ShakeMap-derived ground motion estimates, EQLs, road access disruption, and local geological conditions.

5.4.1. Community mosques

Twenty–one community–built, non–heritage mosques located 17–58 km from the epicentre were assessed during the field investigation. These structures represent typical community mosques serving local settlements and should be distinguished from the historic monumental mosques discussed in Section.6.5. Their locations and associated damage grades are shown in Fig. 29. Compared with residential structures in the same settlements, mosques generally exhibited lower damage levels, which may reflect improved construction quality and workmanship, as these buildings are often funded and supervised by local communities. Generally, in contrast to residential buildings of similar typologies (Section 5.3), full out–of–plane infill failures and roof collapses were not prevalent. Damage was instead dominated by severe diagonal and X-shaped shear cracking accompanied by localised crushing and spalling. This can be demonstrated in Fig. 30a and b for mosques constructed of CM with CMU infills (Fig. 30), where the observed damage is consistent with the in–plane shear crack pattern previously identified for residential buildings (Figs. 25 and 26). Some mosques consisted of CM frames with traditional SM infill panels (Fig. 30c). Damage patterns included plaster detachment, diagonal shear cracking, and horizontal cracks along panel edges, indicating weak frame–infill interaction and insufficient confinement. This structural response is consistent with construction sequences in which RC frames are erected first and subsequently infilled with stone masonry panels, as described in Section 5.3.4 (Fig. 27). Traditional mosques constructed as URM buildings with RE and SM exhibited damage associated with limited interlocking of masonry units, poor mortar quality, and weak wall-to-wall and wall-to-roof connections, similar to the behaviour discussed for residential URM buildings (Section 5.3.2). The most common failures involved partial collapse of external load-bearing walls and out–of–plane mechanisms (Fig. 30d and e), generally followed by arch–shaped cracking at wall heads indicating masonry leaf separation and localised material loss, likely triggered by timber roof beam impact and thrust effects during seismic loading (Fig. 30). Additionally, diagonal shear cracking was observed in internal load–bearing walls (Fig. 30f and g), and opening corner cracks were also common (Fig. 30h), along with floor cracking (Fig. 30i and j) that reflected combined in–plane action.

A common structural feature of the surveyed mosques was the presence of slender square-shaped minarets, typically constructed as RC frame structures that act as vertically independent elements. However, the absence of adequate seismic separation joints resulted in pounding interactions with adjacent prayer halls (Fig. 30k), as the slender minaret structures and the main mosque buildings exhibit different dynamic responses during seismic excitation. This interaction was evidenced by vertical interface cracking and shear damage in adjacent infill panels; however, no global collapses were observed. The most severe damage involved partial failure of unconfined upper parapets lacking continuous tie beams (Fig. 30l), and shear cracking in the infill panels along the upper minaret shafts (Fig. 30m). In several cases, local repair and stabilisation measures had already been implemented to address pounding–related and shear–induced damage (Fig. 30n and o).



Fig. 30. CM mosques with CMU infill panels showing: (a–b) severe diagonal and X-shaped widespread shear cracking and partial collapse of infill panels; CM mosques with SM infill panels showing: (c) diagonal and horizontal infill separation cracks along with plaster detachment, indicating poor frame–infill interaction; URM mosques with RE and SM showing: (d–e) partial collapse of external walls, (f-g) diagonal shear cracking of internal walls, (h) opening corner cracks, (i-j) floor cracks; Minarets showing: (k) pounding damage; (l) partial collapse of unreinforced upper parapets; (m) diagonal shear cracking of infill panels; (n–o) repair interventions.

5.4.2. Other Non–Residential buildings

Field observations also included commercial buildings, schools, healthcare facilities, and hotels. Seven healthcare facilities were inspected externally only, as access was not authorised during the mission. RC frame and CM buildings with CMU infill generally

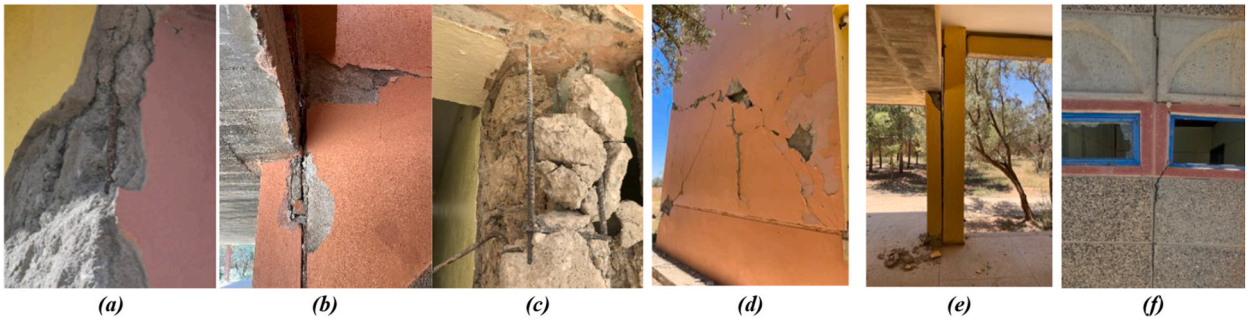

Fig. 31. (a) Concrete spalling; (b) separation between infill panel and RC frame; (c) possible column hinges with insufficient reinforcement confinement; (d) shear cracking and CMU block loss in infill panels; (e) residual drift in adjacent RC framed structures; (f) prefabricated concrete classroom showing panel separation and localised damage.

performed satisfactorily and remained operational, with damage limited to DG1, typically consisting of hairline or minor diagonal cracks in infill panels. In contrast, the only traditional SM facility experienced DG4, characterised by shear cracking in load–bearing masonry walls.

Seven schools were inspected and were predominantly RC moment–frame structures with CMU infills and RC slabs. Damage ranged from DG1 to DG3, including plaster cracking and concrete spalling exposing the steel reinforcement (Fig. 31a), pounding damage between adjacent buildings (Fig. 31b), possible column hinging with insufficient reinforcement confinement (Fig. 31c), and shear cracks in infill panels (Fig. 31d). Residual drifts were also evident in some buildings as shown in Fig. 31e for two adjacent RC framed structures. In some cases, damage was associated with structural irregularities such as soft–storey configurations or buildings constructed on sloping terrain. Schools built with precast concrete panels generally performed better, although limited panel displacement and localised damage were observed (Fig. 31f) in addition to roof damage due to inadequate roof–to–wall connections (Fig. 31).

Hotel buildings showed mixed performance, however, most remained operational and sustained only limited damage. Three hotels were inspected in detail. The most severe case involved a four–storey RC frame hotel constructed on a slope that experienced a soft–storey collapse (DG5), resulting in partial structural failure (Fig. 32a). A second three–storey RC frame hotel with hollow clay brick infill experienced DG2, mainly non–structural damage, including detached rendering and diagonal cracks in panels (Fig. 32b and c). A traditional RE riad exhibited DG3, with shear cracking in external and internal walls and damage associated with inadequate roof–to–wall connections. While hotels are generally built and maintained to meet accreditation standards and guest expectations, their relatively rapid recovery may have been influenced by owners prioritising reopening over accessing government stipends, particularly where projected revenues exceeded available subsidies. This may explain why performance indicators were not readily traceable during the field mission.

A total of 29 commercial buildings were inspected, exhibiting a wide range of structural typologies, including RC frames, CM with CMU infill, and URM construction. Most buildings experienced DG1–DG3, typically characterised by plaster cracks, infill damage, and separation between frames and panels. However, several cases of DG4–DG5 were observed, particularly in RC frame buildings affected by structural irregularities such as soft–storey configurations, re–entrant plan geometries, or construction on sloping terrain. URM buildings showed damage associated with weak connections and heavy roof systems. Two complete collapses of commercial marketplaces were documented. Fig. 32d shows an RC frame building from the 1930s where one portion collapsed due to inadequate reinforcement and confinement detailing, while the adjacent portion remained standing but exhibited severe column shear failure, likely associated with torsional response due to asymmetric lateral stiffness. Another collapse case is shown in Fig. 32e, where debris similarly revealed poor reinforcement detailing and inadequate confinement.

6. Cultural heritage damage and conservation response

Designated cultural heritage assets known to have sustained earthquake damage were inspected during the field reconnaissance, with site selection informed by the preliminary post-earthquake assessments undertaken by the Moroccan Ministry of Youth, Culture and Communication, together with logistical considerations and the field itinerary [5–7]. Following the methodology described in Section 2.2, the EEFIT mission inspected nine protected heritage sites dating from the 12th to the 19th century that sustained earthquake damage across the provinces of Marrakech, Al Haouz, Ouarzazate, and Taroudant (see Table 2). The resulting georeferenced observations were incorporated into the common multi-layer geospatial framework as the cultural heritage layer (Fig. 29). This layer is interpreted alongside the complementary thematic layers, enabling the observed heritage damage to be evaluated in the context of regional ShakeMap-derived ground motion estimates, EQLs, local geological conditions, and the performance of the surrounding building stock.

The monuments are primarily constructed using traditional Earthen materials (E), including RE and adobe, or SM in the form of load–bearing walls with timber floors and roofs. Consequently, they share many construction characteristics with the traditional URM residential building stock described in Section 5.3.2. Field observations indicated that many of the designated heritage monuments exhibited higher standards of historical craftsmanship together with evidence of previous conservation and maintenance interventions. However, the pre-earthquake state of conservation varied between sites, ranging from recently restored monuments to structures showing more limited maintenance. The assessment of these monuments therefore provides a complementary perspective

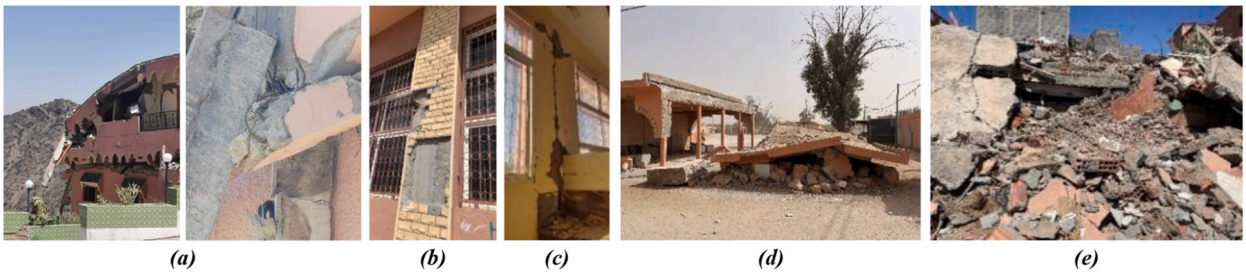

Fig. 32. (a) Four–storey RC hotel exhibiting a soft–storey collapse; (b–c) three–storey RC frame hotel showing external and internal non–structural damage; (d) RC frame commercial building with full collapse, while the adjacent structure remains intact due to sufficient lateral stiffness; (e) RC frame commercial building showing total collapse with debris indicating poor reinforcement detailing and inadequate confinement.

Table 2
Inspected monuments, reported Modified Mercalli Intensity (MMI) intensity and observed damage level.

Monument	Province	Epic. Dist. (km)	Max. MI [1]	Date	URM	Damage
Koutoubiya Mosque	Marrakech	~72	7.8	12th c.	SM	DG2
El Badi Palace	Marrakech	~72	7.8	16th c.	RE	DG3
Saadian Tombs	Marrakech	~72	7.8	16th c.	RE	DG3
Bahia Palace	Marrakech	~72	7.8	19th c.	Mixed	DG4
Marrakesh Wall	Marrakech	~72	7.8	12th c.	RE	DG3
Tinmel Mosque	Al Haouz	~30–35	9.1	12th c.	RE	DG5
Aït Ben Haddou	Ouarzazate	~125	5.9	17th c.	E, SM	DG4
Kasbah Taourirt	Ouarzazate	~130	5.9	18th c.	E	DG3
Taroudant Wall & Babs	Taroudant	~95	6.1	12th –16th c.	RE	DG3

on the seismic performance of traditional URM construction by illustrating the influence of construction quality and pre-earthquake conservation on observed earthquake damage. Observed damage ranged from DG2 to DG5, with most monuments experiencing DG3, typically manifested as seismic crack patterns and localised structural failures. The most severe damage occurred at Tinmel Mosque (DG5), which experienced partial structural collapse (Sec 6.5).

6.1. *Immediate response: consolidation and early repair of protected heritage sites*

Site inspections indicate that Moroccan authorities rapidly implemented stabilisation measures at damaged heritage sites. Temporary propping and shoring were widely used to stabilise walls and structural elements while conservation strategies were being developed. For example, extensive timber shoring supported the remaining walls of Tinmel Mosque (Fig. 42f). While steel propping was installed in the central courtyard of the Large Riad at Bahia Palace (Fig. 33a).

Similar interventions were observed along the RE city walls of Marrakech and Taroudant, where bastions were stabilised using horizontal timber boards stitched through the walls to control vertical cracks (Fig. 33b–d). Site observations suggest that conservation responses generally relied on traditional materials and techniques, consistent with international conservation principles for historic structures [99].

The urgency of these interventions reflects the strategic importance attributed by the Moroccan authorities to cultural heritage, not only as a repository of cultural value but also as a key driver of tourism, a sector contributing more than 7% of Morocco's GDP [5]. This is exemplified by the reopening of various affected heritage sites to visitors within one month of the earthquake, including major monuments in the World Heritage Site of the Medina of Marrakech [7].

In several locations, earlier restoration interventions using compatible materials were evident, such as previous repairs along the Taroudant city wall (Fig. 34). In some cases, post–earthquake repairs had already begun during the EEFIT mission, including crack stitching with timber poles embedded in earthen mortar at Kasbah Taourirt (Fig. 35). The conservation approach applied to monumental architecture contrasts with the more limited and often ad hoc maintenance practices observed in residential buildings constructed with traditional materials. Although some URM structures incorporate traditional mitigation measures such as timber ties, dowels, or cornerstones (Fig. 21e and 23), these elements were often irregularly implemented or poorly anchored, limiting their effectiveness.

The following case studies illustrate the observed range and extent of damage in different monumental heritage sites affected by the earthquake that have been conserved and repaired using primarily compatible materials.

6.2. *Aït Ben Haddou*

Aït Ben Haddou, a fortified *ksar* recognised as a UNESCO World Heritage Site since 1987, provides an example of earthquake damage in protected earthen settlements. The site comprises earthen buildings constructed along the slopes of a hill and enclosed within defensive walls. Its authenticity is preserved through conservation and management measures that promote the continued use of traditional materials and construction techniques [62]. At the time of inspection, the site exhibited low–to–moderate damage. Extensive spalling of earthen render was observed, particularly around corners and openings in taller buildings, although more generalised render failure occurred in some structures, possibly where the state of conservation was poorer (Fig. 36). Corner separation cracks associated with out–of–plane wall behaviour and spalling around openings were also recorded (Fig. 37a and b), while diagonal shear cracks around openings were also frequently recorded (Fig. 37c and d). Local failures occurred in some buildings, with repairs underway. Piles of reconstruction materials were observed on site, including E blocks for rebuilding damaged elements, alongside some cement blocks (Fig. 38).

6.3. *Bahia Palace*

Bahia Palace is a 19th–century complex located within the Medina of Marrakech World Heritage Site. Constructed in two phases during the 1860s and 1890s under the patronage of Moussa Ben Ahmed El Boukhari and his son Ahmed Ben Moussa [100], the complex comprises courtyards, riads, gardens, and associated structures built primarily of masonry walls with timber floor and roof systems.

Prior to the earthquake the palace was in generally good condition following several restoration campaigns undertaken during the



Fig. 33. Propping and consolidation interventions: (a) Central courtyard of Large Riad, Bahia Palace, Marrakech; (b) Marrakech city wall bastion; (c) Taroudant city wall bastion, external view; (d) Taroudant wall bastion, internal view.

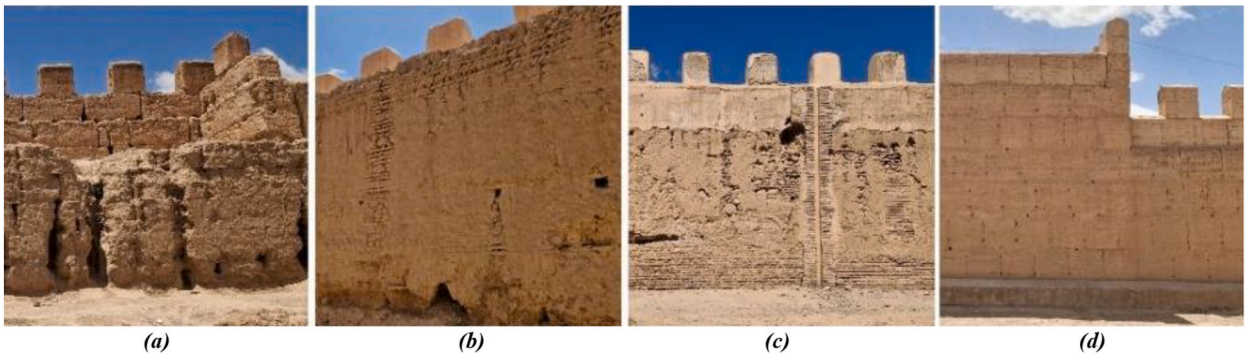

Fig. 34. Diverse states of conservation and past restoration interventions along the city wall of Taroudant.

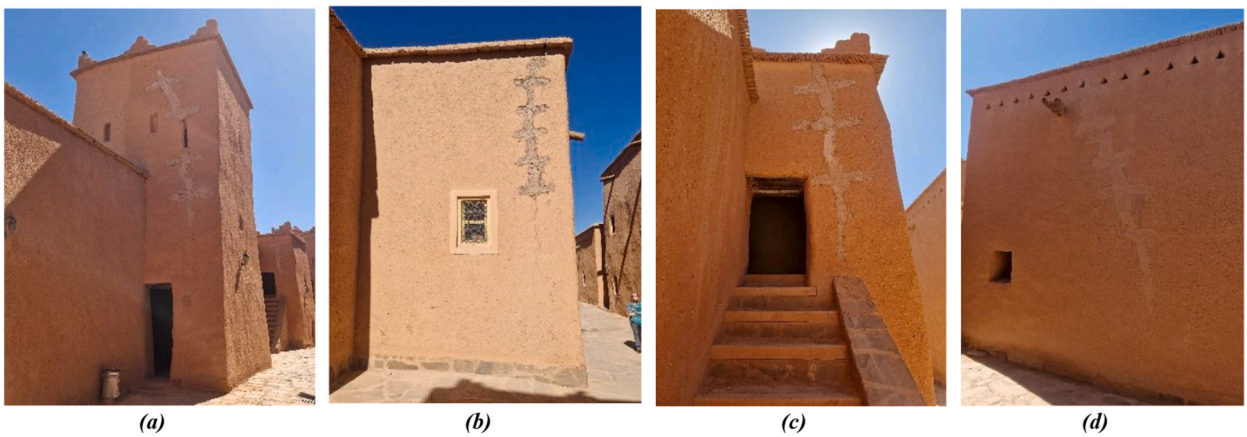

Fig. 35. Post–earthquake crack stitching interventions at Kasbah Taourirt, Ouarzazate.

past century. The earthquake caused moderate to significant damage across the complex, which remained closed to visitors for one month before reopening on 8 October 2023 together with other major tourist sites [7]. Local collapses were mainly observed in taller structures, roof parapets, and corners, with the most significant failure occurring at the roof of the large pavilion in the Courtyard of Honour (Fig. 39a). In–plane shear cracks were recorded around openings and corners (Fig. 39b and c), while separation of orthogonal walls produced vertical corner cracks in several areas (Fig. 39d). The Large Riad exhibited extensive out–of–plane and shear cracking along the central courtyard (Fig. 33a) and remained closed to visitors. Temporary stabilisation measures, including propping and scaffolding, were installed during the early conservation response (Figs. 33a and. 39a).



Fig. 36. Aït Ben Haddou: (a–c) Spalling of earthen render around corners and openings.

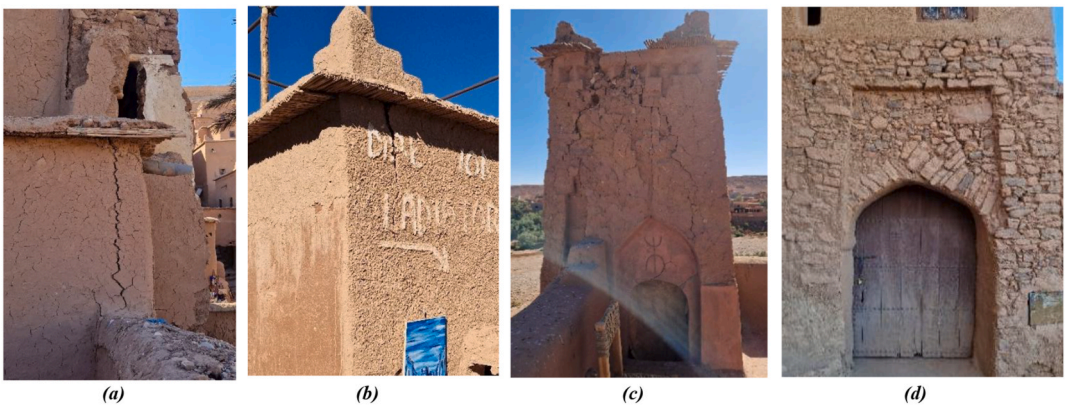

Fig. 37. Aït Ben Haddou: (a–b) Corner separation cracks indicating out–of–planes failure (c–d) diagonal shear cracks to openings.

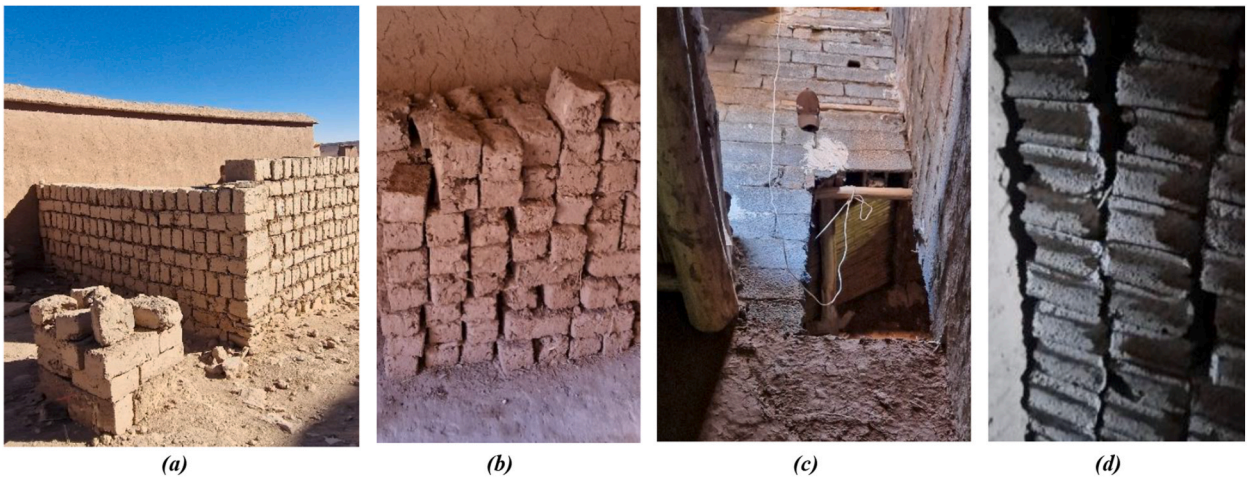

Fig. 38. Aït Ben Haddou: post–earthquake rebuilding materials: (a–b) adobe blocks; (c–d) cement blocks.

6.4. Taroudant city wall

The Taroudant city wall, an approximately 8 km–long defensive ramparts constructed between the 12th and 16th centuries, represents one of the most extensive rammed–earth fortifications in Morocco [101]. Prior to the earthquake, the wall displayed

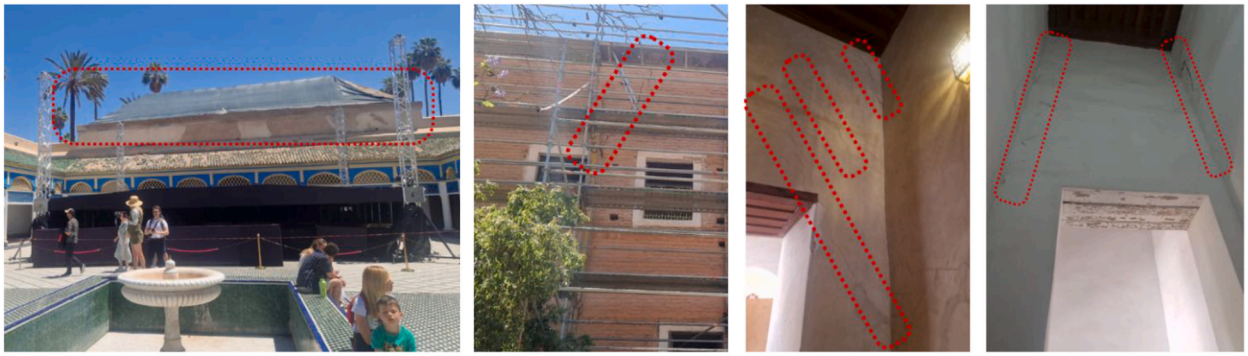

Fig. 39. Bahia Palace: (a) failure of roof of large pavilion at the Courtyard of Honour; (b–c) diagonal shear cracks at various locations; (d) corner cracks at top of walls.

heterogeneous conservation conditions along its length due to repairs undertaken during different historical periods (Fig. 34).

Earthquake damage ranged from minor seismic cracking to failure, with the extent of damage influenced by several factors, including wall orientation relative to the direction of shaking (in–plane versus out–of–plane), wall height and stiffness, state of conservation, and the characteristics of past conservation interventions. Vertical cracks at or near corners were frequently observed at bastions along the western stretch of the rampart, where the wall was subjected to out–of–plane motion.

These cracks followed construction joints between rammed-earth panels (Fig. 40a and b). Material crumbling and toe crushing at the base of the wall under out-of-plane loading (Fig. 40c), as well as the reopening of previously repaired cracks under both in-plane and out-of-plane loading (Fig. 40d), were also observed. These damage patterns highlight the behaviour of earlier repair interventions using traditional techniques, such as masonry rebuilding with soft mortar or the use of timber keys across cracks. At the time of the EEFIT inspection, several sections had already been temporarily stabilised through propping (Fig. 33c and d). The *Babs*, or gates of the wall, also exhibited notable seismic damage., including out–of–plane cracking at the base of merlons at Bab Targhount and vertical corner cracks with partial parapet collapse at Bab Ouled Bonouna (Fig. 41).

6.5. *Historic mosques*

Historic mosques in Marrakech and the surrounding areas exhibited varying levels of earthquake damage and subsequent repair interventions [19]. The Kharbouch Mosque sustained significant structural damage and was undergoing stabilisation and repair works during the EEFIT inspection. Follow–up observations indicate that the structure is currently under partial reconstruction as part of ongoing restoration efforts (Fig. 42a and b).

In contrast, major monuments such as the Koutoubia Mosque remained largely intact, although conservation works were observed on the minaret (Fig. 42c and d). Previous reconnaissance studies [18] reported cracking in the upper portion of the 77 m minaret and

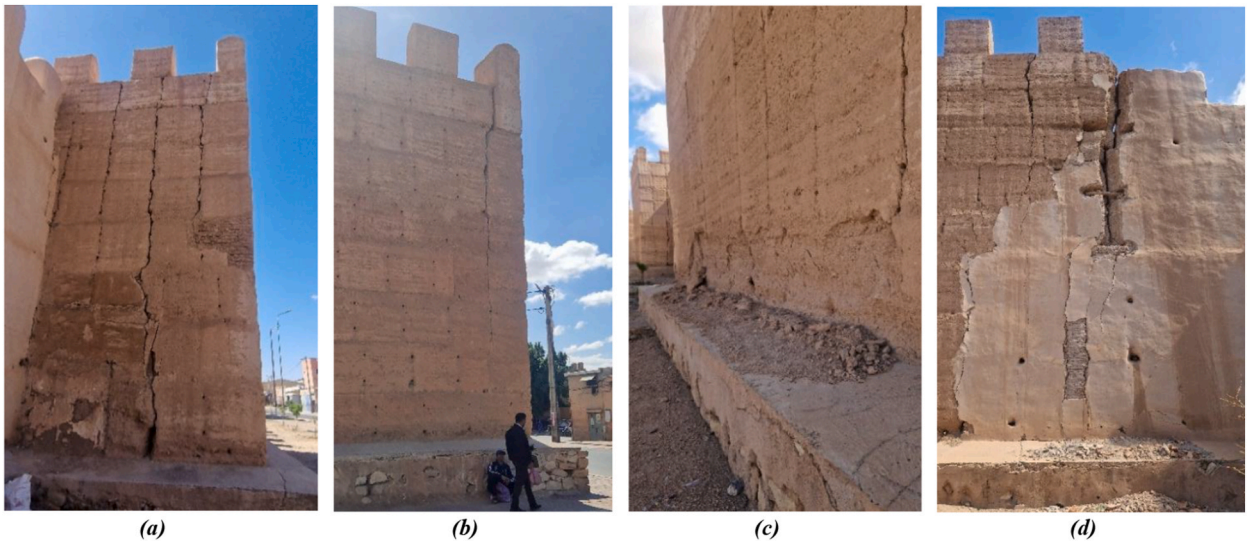

Fig. 40. Taroudant city wall: (a–b) vertical cracks at or near corners; (c) toe crushing at the wall base; (d) reopening of past crack repairs.



Fig. 41. Babs of Taroudant city wall: (a) out–of–plane cracks at the base of merlons at Bab Targhount; (b) vertical corner cracks at Bab Ouled Bonouna; (c) partial collapse at the top of the wall at Bab Ouled Bonouna.



Fig. 42. Historic mosques affected by the 2023 Al Haouz earthquake: (a–b) Kharbouch Mosque inspected during the EEFIT mission in 2024 and during a follow–up visit in December 2025; (c–d) Koutoubia Mosque inspected during the EEFIT mission in 2024; (e) conservation interventions observed on the Koutoubia minaret in December 2025; (f) Tinmel Mosque showing extensive temporary interventions.

the installation of temporary steel bracing after the earthquake to stabilise the structure. The mosque was reopened to the public in September 2025 following conservation works, although monitoring and minor repair interventions continue (Fig. 42e). The Tinmel Mosque, located in the High Atlas Mountains, experienced the most severe damage among the inspected religious monuments. This 12th-century Almohad structure suffered major structural collapse during the earthquake. Its severe damage is likely to reflect the combined effects of its close proximity to the epicentre and the associated high levels of ground shaking, together with its structural configuration and the ongoing restoration works at the time of the event, including the presence of scaffolding throughout parts of the site [6]. Temporary stabilisation measures and reconstruction work have since been initiated. These observations highlight the varying seismic responses of historic mosques depending on their proximity to the earthquake source, structural configuration, construction materials, and pre-earthquake conservation conditions.

7. Conclusions

This study presents a multi-layer post-earthquake reconnaissance framework that combines five complementary remote sensing (RS) with systematic engineering field observations within a common geospatial framework. The resulting multi-layer geospatial dataset comprises complementary thematic layers, including regional-scale RS observations, earthquake-induced landslides (EQLs), road accessibility, residential and non-residential building assessments with EMS–98 damage classifications, and cultural heritage investigations. Organised within a common spatial framework, these complementary layers enabled earthquake impacts to be interpreted consistently across regional, settlement, and asset scales, linking regional patterns of disturbance with the engineering processes responsible for the observed damage. This multi-layer farmwork, therefore provided a means of examining different, but interconnected, consequences of the earthquake-induced hazards, including regional disturbance, landslides, accessibility disruption, structural performance, and cultural heritage. By combining regional and local-scale observations, the framework helped identify where earthquake impacts occurred and explain the factors contributing to differences in their severity and distribution, providing engineering insights that neither RS nor field reconnaissance could have achieved independently.

The combined use of SAR-based Damage Proxy Maps, Nighttime Light data, and Normalised Difference Vegetation Index filtering enabled the rapid identification of settlements exhibiting different levels of regional disturbance, supporting the prioritisation of field reconnaissance. However, these regional-scale products alone could not explain the causes of the observed damage. Systematic engineering investigations provided complementary information unavailable from RS, including damage severity, structural failure mechanisms, construction practices, and the influence of local geological and site conditions. Conversely, the RS products placed these detailed observations within their broader spatial context, enabling local damage patterns to be interpreted in relation to regional earthquake impacts and supporting a more representative assessment of seismic performance across the affected region. Importantly, the regional screening also ensured that settlements exhibiting lower levels of disturbance were included, allowing earthquake performance to be evaluated across a broader spectrum of damage conditions rather than only the most severely affected locations. Thus, the integration of regional RS screening with systematic field observations provided both a means of efficiently targeting reconnaissance and a broader spatial context for interpreting detailed engineering observations.

A total of 2671 landslides were identified, with their spatial distribution strongly controlled by topography and local geological conditions. While the landslide inventory documented the extent of slope failures, their principal consequences became clearer when the regional EQL observations were interpreted together with the road damage and accessibility observations recorded during the field reconnaissance. Landslides were concentrated along the principal mountain valleys, which also contain the main transport corridors serving remote settlements. Field observations confirmed that landslide debris, rockfalls, failures of engineered slopes, and other geotechnical damage resulted in road blockages and restricted access along these routes. Consequently, the significance of the landslides was not determined solely by their number or size, but also by their location within a road network on which remote communities depend. These disruptions constrained emergency response, reconnaissance activities, road-clearance operations, and the delivery of humanitarian assistance. In contrast, the building surveys demonstrated that structural damage within these settlements was primarily associated with seismic shaking rather than direct landslide impacts. Interpreting the EQL inventory together with the field observations of road disruption therefore revealed a different consequence of the earthquake from that captured by the building assessments: landsliding primarily affected accessibility, whereas seismic shaking governed the distribution and severity of structural damage. This demonstrates the added value of interpreting the regional landslide inventory together with systematic field observations of infrastructure impacts rather than considering the landslide inventory in isolation.

The integration of the building observations with the regional RS and ShakeMap-derived ground-motion information further demonstrated the importance of combining regional and asset-scale observations. The systematic assessment of 455 buildings showed that, although confined masonry (CM) and reinforced concrete (RC) buildings generally exhibited lower damage grades than traditional unreinforced masonry (URM) and hybrid buildings, seismic performance varied considerably within each structural typology. Buildings of the same structural typology located within areas exhibiting similar levels of RS-derived disturbance and comparable regional ShakeMap ground-motion estimates frequently experienced markedly different damage levels. Because local site effects remain uncertain owing to the limited availability of instrumental recordings, and the lack of reliable Vs,30 maps for the High Atlas region, these regional ground-motion estimates and RS-derived disturbance patterns alone could not fully explain the observed variability in seismic performance. Instead, the field investigations demonstrated that construction quality, structural detailing, material properties, continuity of the load path, maintenance, and local geological conditions were equally important in governing the observed damage. The combined interpretation therefore showed where regional-scale indicators were insufficient to explain local structural performance and highlighted the importance of detailed engineering observations for understanding the mechanisms underlying observed damage.

The assessment of cultural heritage within the same geospatial framework highlighted the distinct vulnerabilities and recovery requirements of historic assets compared with the wider building stock. Although predominantly constructed using traditional materials and generally sustaining moderate damage, with localised severe cases such as the Tinmel Mosque, the observed performance reflected the influence of prior maintenance, construction quality, and conservation practices. The emergency interventions documented during the reconnaissance, which largely adopted compatible materials and traditional stabilisation techniques, demonstrate that post-earthquake recovery strategies for cultural heritage require intervention approaches distinct from those applied to the wider building stock, recognising both the structural characteristics and the cultural and socio-economic significance of these assets. The integration of cultural heritage observations within the wider earthquake-impact assessment therefore allowed the vulnerability and recovery requirements of historic assets to be considered alongside, but distinguished from, those of the general building stock.

More broadly, this study demonstrates the value of organising complementary RS products and systematic engineering field observations within a common multi-layer geospatial framework. The added value lies not in requiring direct spatial or statistical relationships between every dataset, but in enabling distinct but interconnected earthquake consequences to be interpreted within a common spatial context. The framework links regional disturbance with observed infrastructure disruption, structural performance, and heritage vulnerability, while allowing the limitations of regional-scale indicators to be identified through detailed field observations. This integrated approach provides a more comprehensive understanding of earthquake impacts across regional, settlement, and asset scales than could be achieved through RS analysis or field reconnaissance alone.

Building on these insights, and informed by stakeholder engagement activities (Section 2.4), which helped contextualise the results in relation to practical needs and reconstruction priorities, the following evidence-based recommendations are proposed for future research, practice, and implementation in similar mountainous and resource-constrained contexts.

- **Multi-hazard, road disruption, and site conditions.** The multi-layer post-earthquake assessment showed that earthquake-induced landslides primarily disrupted road access rather than directly causing widespread structural damage. Future work should extend this framework through explicit cross-layer analyses to examine how hazard impacts, road accessibility, building damage, and community functionality interact and influence post-earthquake recovery. This could include synthesis matrices linking field observations with RS-derived indicators and other spatial datasets, supporting improved understanding of earthquake impacts and the development of scalable, data-driven methods for rapid post-earthquake assessment in data-scarce and inaccessible environments.
- **Construction practices and capacity building.** The assessment of 455 buildings demonstrated that construction quality and structural detailing influenced seismic performance more strongly than structural typology alone. Recurrent deficiencies such as inadequate wall-to-roof connections, discontinuous load paths, poor reinforcement detailing, and poor-quality construction materials governed the dominant failure mechanisms. These findings emphasise the need for targeted training and capacity building for masons, contractors, and local builders, particularly in rural areas where informal and incremental construction is prevalent.
- **Context-specific construction solutions.** The observed variability in seismic performance within the same structural typologies demonstrates that reconstruction guidance should be tailored to the specific vulnerabilities of traditional masonry, hybrid, and other non-engineered buildings. RC, often introduced into traditional systems, should not be considered a universal solution but should be integrated only where compatible with local construction practices, available skills, and materials.
- **Role of local context and co-production.** The observed variability in construction quality, maintenance, and structural detailing highlights the importance of understanding how buildings are constructed, modified, and maintained within specific social and economic contexts, and should be developed through co-production with local communities and stakeholders.
- **Heritage conservation and resilience.** The observed performance of heritage structures highlights the importance of maintenance, construction quality, and conservation practices in reducing seismic vulnerability. Post-earthquake interventions should prioritise the use of compatible materials and traditional stabilisation techniques, while recognising the socio-economic value of heritage assets, including their role in supporting local tourism.
- **Data integration and digital tools.** The multi-layer geospatial evidence base developed in this study demonstrates the value of combining systematic field observations with very-high-resolution satellite imagery. Future work should build on this approach by generating labelled datasets that link ground-based damage assessments with RS products, supporting improved damage classification and the advancement of scalable, data-driven methods for rapid post-earthquake assessment in data-scarce and inaccessible environments.
- **Reconstruction and future research.** Future efforts should focus on developing context-specific reconstruction guidelines for traditional masonry, hybrid, and other non-engineered buildings, informed by the dominant vulnerability characteristics and failure mechanisms identified during this study. These should be complemented by expanded data collection in underrepresented seismic regions and further development of integrated RS and field-based approaches to support rapid post-earthquake assessment, risk reduction, and resilient recovery.

The integrated multi-layer reconnaissance framework developed in this study provides a structured and reproducible workflow for post-earthquake assessment that can be adapted to other remote, data-scarce, and multi-hazard-prone regions. While the overall workflow provides a structured and reproducible methodology, its implementation should be tailored to the local context, considering the availability of RS data, accessibility constraints, geomorphological setting, and local construction practices. Adapting the reconnaissance strategy to these regional characteristics will maximise the value of the integrated framework for supporting informed, risk-aware decision-making and resilient recovery.

CRediT authorship contribution statement

Viviana Iris Novelli: Writing – review & editing, Writing – original draft, Visualization, Validation, Supervision, Software, Resources, Project administration, Methodology, Investigation, Funding acquisition, Formal analysis, Data curation, Conceptualization. **Fabio Freddi:** Writing – review & editing, Writing – original draft, Visualization, Validation, Supervision, Software, Resources, Project administration, Methodology, Investigation, Funding acquisition, Formal analysis, Data curation, Conceptualization. **Michael Whitworth:** Writing – review & editing, Writing – original draft, Visualization, Validation, Supervision, Software, Resources, Project administration, Methodology, Investigation, Funding acquisition, Formal analysis, Data curation, Conceptualization. **Martin Stokes:** Writing – review & editing, Writing – original draft, Visualization, Validation, Software, Investigation, Formal analysis, Data curation. **Alaeddine Belfoul:** Writing – review & editing, Writing – original draft, Validation, Investigation, Data curation, Conceptualization. **Sarah Esper:** Writing – review & editing, Writing – original draft, Visualization, Validation, Software, Investigation, Formal analysis, Data curation. **Riccardo Vitale:** Writing – review & editing, Writing – original draft, Visualization, Software, Investigation, Formal analysis, Data curation. **Zeyad Khalil:** Writing – review & editing, Writing – original draft, Visualization, Validation, Software, Investigation, Formal analysis, Data curation. **Mauritz Feldbrugge:** Writing – review & editing, Software, Investigation, Formal analysis, Data curation. **Asmaa Maaroufi:** Writing – review & editing, Investigation, Data curation. **Hiba Shaimed:** Investigation. **Hamza Skikra:** Investigation. **Alejandra Albuerne:** Writing – review & editing, Writing – original draft, Visualization, Validation, Investigation, Data curation. **Marco Redaeli:** Investigation. **Giorgia Giardina:** Writing – review & editing, Supervision, Methodology, Investigation, Funding acquisition, Data curation, Conceptualization. **Keith Adams:** Investigation. **Roberto Gentile:** Writing – review & editing, Writing – original draft, Validation, Investigation. **Siau Chen Chian:** Investigation. **Sarah J. Boulton:** Writing – review & editing, Visualization, Validation, Software, Data curation. **Joshua Jones:** Writing – review & editing, Visualization, Validation, Software, Formal analysis. **Pietro Milillo:** Writing – review & editing, Validation, Supervision, Data curation. **Fatemeh Foroughnia:** Writing – original draft, Validation, Data curation. **Valentina Putrino:** Writing – review & editing. **Jacob Black:** Investigation.

Funding

This work was supported by NE/Y006356/, AECOM and the TU Delft Safety & Security Institute.

Declaration of competing interest

The authors declare the following financial interests/personal relationships which may be considered as potential competing interests: Viviana Iris Novelli reports financial support and travel were provided by Cardiff University. Giorgia Giardina reports financial support and travel were provided by Delft University of Technology. If there are other authors, they declare that they have no known competing financial interests or personal relationships that could have appeared to influence the work reported in this paper.

Acknowledgements

The authors would like to acknowledge the support and contributions of the following individuals and organisations: ReBuild Initiative: Hassan Kaddouri (Coordinator) and Abdeslem Yahyaoui (Field Expert). Mohammed VI Polytechnic University (UM6P): Khalid Baddou (Chief of Staff, President's Office); Hicham El Habti (President); Hassan Naciry (Project Manager, President's Office); Robin Kurtz (Geology and Sustainable Mining Institute); Kawtar Oukhouya (School of Collective Intelligence); Sarah Alami (School of Collective Intelligence); Zakariae Benchrif (School of Collective Intelligence); and Edmond Seabright (School of Collective Intelligence). Red Cross: Katie Bitten; Mohammed Bashein and Noor Kuchai. Miyamoto International: Ayoub Bellouch; Kit Miyamoto and Yassin Elouardi. Build Change: Louise Foulkes and Pierre Paya. MBLA, Morocco: Abdellah Aghraz and Rachid Aitbabahmad; CARE: Steph Wood; Emerging Business Factory: Taoufik Aboudia, Mohammed V University: Nabil Mekaoui; Ministry of Youth, Culture and Communication of Morocco: Faissal Cherradi; ICOMOS Morocco: Abderrahim Kassou; Global Diversity Foundation: Gary Martin; and Hassan II University, Casablanca, Morocco Dalila Loudyi.

Data availability

Data will be made available on request.

References

[1] USGS, M 6.8 – Al Haouz, Morocco, 2023. Retrieved from, https://earthquake.usgs.gov/earthquakes/eventpage/us7000kufc.
[2] World Bank, Morocco: Mobilizing the Financial Sector for Improved Resilience Against Disasters and Climate Shocks, World Bank Blogs, 2024. Available at: https://blogs.worldbank.org/en/arabvoices/morocco–mobilizing–financial–sector–improved–resilience–against–disasters–and–climate.
[3] I. Bondár, Y. Timoulali, A. Chiang, L. Hni, M. Kasmi, Relocation of the 8 September 2023 high Atlas, Morocco, earthquake aftershock sequence, Bull. Seismol. Soc. Am. (2024), https://doi.org/10.1785/0120240100. N. p., 2024.
[4] W.L. Yeck, A.E. Hatem, D.E. Goldberg, W.D. Barnhart, J.A.T. Jobe, D.R. Shelly, A. Villaseñor, H.M. Benz, P.S. Earle, Rapid source characterization of the 2023 M_w 6.8 Al Haouz, Morocco, earthquake, Seism. Rec. 3 (4) (2023) 357–366.
[5] World Tourism Organization, Tourism Doing Business – Investing in Morocco, UN Tourism, Madrid, 2025. Available at: https://www.untourism.int/investment/tourism-doing-business-investing-in-morocco.

[6] Medias24, 27 Sites Historiques Ont Été Gravement Endommagés Par Le Séisme Du 8 Septembre Selon Un Premier Constat, 2023. Available at: https://medias24.com/2023/09/11/27-sites-historiques-ont-ete-gravement-endommages-par-le-seisme-du-8-septembre/.

[7] Morocco World News, Historical Sites in Earthquake–Hit Areas in Morocco Reopen for Visitors, Morocco World News, 2023. https://www.moroccoworldnews.com/2023/10/28277/historical–sites–in–earthquake–hit–areas–in–morocco–reopen–for–visitors/. (Accessed 9 October 2023).

[8] E.A. Haddad, K. El Aynaoui, A. Ait Ali, M. Arbouch, H. Saoudi, I.F. de Araújo, Assessing the Economic Impacts of Al Haou Earthquake: Damages and Recovery Strategy (No. 1981), Policy Center for the New South, 2024.

[9] FRC, Morocco Earthquake 2023 Operation Update No.5 (12 Months), ReliefWeb, 2024. Available at: https://reliefweb.int/report/morocco/morocco–earthquake–2023–operation–update–5–12–months–mdrma010.

[10] PBS NewsHour, Morocco works brick–by–brick to reconstruct 12th–century mosque destroyed by 2023 earthquake, Available at: https://www.pbs.org/newshour/world/morocco–works–brick–by–brick–to–reconstruct–12th–century–mosque–destroyed–by–2023–earthquake, 2024.

[11] IFRC, 2023 Morocco Earthquake: Emergency Response, Recovery and Reconstruction, ReliefWeb, 2023. Available at: https://reliefweb.int/report/morocco/2023–morocco–earthquake–emergency–response–recovery–and–reconstruction.

[12] British Red Cross, Morocco Earthquake: latest news and updates, British Red Cross (2023). https://www.redcross.org.uk/stories/disasters–and–emergencies/world/morocco–earthquake–2023–latest–news–and–updates.

[13] International Federation of Red Cross and Red Crescent Societies (IFRC), Morocco Earthquake Emergency Response, IFRC, 2023. https://www.ifrc.org/emergency/morocco–earthquake.

[14] International Medical Corps, Responding to the Earthquake in Morocco, International Medical Corps, 2023. https://internationalmedicalcorps.org/emergency–response/morocco/.

[15] United Nations Office for the Coordination of Humanitarian Affairs (OCHA), Morocco: Earthquake Situation Report, United Nations, 2023. https://www.unocha.org.

[16] UK–Med, Concerns for secondary health crisis, as quake–affected people in remote areas of Morocco struggle for help, UK–Med News (2023). https://www.uk–med.org/2023/09/12/secondary–health–crisis–morocco/.

[17] Government of Morocco, World Bank, European Union, and United Nations, Morocco Al Haouz Earthquake: Post-Disaster Needs Assessment (PDNA), World Bank/Global Facility for Disaster Reduction and Recovery, Washington, DC, 2023. https://www.gfdrr.org/en/post-disaster-needs-assessment-pdna.

[18] A. Imtiaz, S. Saloustros, M. Beqiraj, G. Cortés, M. Devaux, E. Lattion, Y. Zhu, H. Sehaqui, Understanding building damage through the lens of the Swiss post–seismic reconnaissance mission of 2023 Al Haouz, Morocco, earthquake, Sci. Rep. 15 (1) (2025) 16587.

[19] L. Taoufiq, M. Chourak, F. Arrakhiz, Structural failure of reinforced concrete buildings: the case of Al Haouz earthquake on 8 September 2023, Morocco, Structures 75 (2025) 108747.

[20] K. Bennis, K. Benazzi, Navigating natural disaster disruption in the hospitality sector: insights from the September 8, 2023, earthquake in Morocco, IDRiM Journal 14 (2) (2024).

[21] B. González–Rodrigo, L. Navas–Sánchez, J.G. Rejas–Ayuga, O. Hernández–Rubio, M.B. Benito, Preliminary geospatial and in situ reconnaissance of the 8 September 2023 Moroccan Atlas earthquake damage, Buildings 14 (3) (2024) 693.

[22] A. Ziraoui, B. Kissi, H. Aaya, N. Mrabet, I. Azdine, Seismic risk assessment, damage estimation, and strengthening of seismic construction standards in Morocco, Journal of Building Pathology and Rehabilitation 9 (1) (2024) 79.

[23] A. Ziraoui, B. Kissi, H. Aaya, I. Azdine, Monitoring seismic activity and implementing risk reduction strategies in Morocco, International Journal on Engineering Applications 12 (4) (2024) 261–269.

[24] Miyamoto International, Morocco earthquake – situational report #1: initial impact assessment. https://miyamotointernational.com/2023–morocco–earthquake–situational–report–1/, 2023.

[25] Miyamoto International, Morocco earthquake – situational report #2: latest situation update. https://miyamotointernational.com/2023–morocco–earthquake–situation–report–2/, 2023.

[26] M. Bao, M.I. Abdelaal, M. Saleh, M. Chourak, M. Mohamed, M. Xing, Unlocking the hidden secrets of the 2023 Al Haouz earthquake: Co-seismic model reveals intraplate reverse faulting in Morocco derived from SAR and seismic data, Int. J. Appl. Earth Obs. Geoinf. 137 (2025) 104420.

[27] S. El Janous, A. El Ghoulbzouri, Evaluation of the seismic susceptibility in the north of Morocco considering the soil–structure interaction, Iranian Journal of Science and Technology, Transactions of Civil Engineering 49 (1) (2025) 547–563.

[28] V.G. Bondur, T.N. Chimitdorzhiev, A.V. Dmitriev, The induced seismicity effect in Morocco caused by a reduced aquifers volume according to Stacking–InSAR method and gravimetric data, Dokl. Earth Sci. 517 (1) (2024) 1269–1275.

[29] D. Cheloni, N.A. Famiglietti, C. Tolomei, R. Caputo, A. Vicari, The 8 September 2023, M_w 6.8, Morocco earthquake: a deep transpressive faulting along the active high Atlas mountain belt, Geophys. Res. Lett. 51 (2) (2024) e2023GL106992.

[30] S. Holail, T. Saleh, X. Xiao, A.H. Ali, D. Li, Building damage detection with UNet–Backbone fusion in high–resolution satellite imagery: 2023 Morocco earthquake, Int. Arch. Photogram. Rem. Sens. Spatial Inf. Sci. (2025) 589–595. XLVIII-G-2025.

[31] A. Habib, I. Berrada, A. El Adnani, Y.A. Laaziz, A. Fadili, A. Lagnaoui, A. Najih, T.Y. Arrad, DInSAR analysis of ground deformation induced by the 2023 Al Haouz earthquake, Morocco, The International Archives of the Photogrammetry, RS and Spatial Information Sciences 48 (2025) 127–131.

[32] N. Fang, Z. Chen, L. Zhao, K. Sun, L. Xie, W. Xu, Joint inversion of InSAR and seismic data unveiling the dynamic rupture process and seismotectonic kinematics of the 2023 M_w 6.8 Morocco earthquake, Remote Sens. 17 (17) (2025) 2971.

[33] K. Huang, G. Wei, K. Chen, N. Zhang, M. Li, L. Dal Zilio, The 2023 M_w 6.8 Morocco earthquake: a lower crust event triggered by mantle upwelling? Geophys. Res. Lett. 51 (12) (2024) e2024GL109052.

[34] A. Najim, Y. Timoulali, M. El Hilali, K. Diani, Geological mapping from satellite imagery and lineament detection in the Imilchil–Aghbala region (High Atlas central and Middle Atlas ridges zone, Morocco), Euro–Mediterranean Journal for Environmental Integration 9 (2) (2024) 875–889.

[35] W. Wu, Y. Zhang, X. Hao, J. Liu, The source kinematics and slip distribution of the 2023 M_w 6.8 Morocco earthquake, J. Afr. Earth Sci. 220 (2024) 105451.

[36] S.M. Wilkinson, J.E. Alarcon, R. Mulyani, J. Whittle, S.C. Chian, Observations of damage to buildings from M w 7.6 Padang earthquake of 30 September 2009, Nat. Hazards 63 (2) (2012) 521–547.

[37] S. Tallett-Williams, B. Gosh, S. Wilkinson, C. Fenton, P. Burton, M. Whitworth, S. Datla, G. Franco, A. Trieu, M. Dejong, V. Novelli, Correction to: site amplification in the Kathmandu Valley during the 2015 M7. 6 Gorkha, Nepal earthquake, Bull. Earthq. Eng. 18 (13) (2020), 6117-6117.

[38] F. Freddi, V. Novelli, R. Gentile, E. Veliu, S. Andreev, A. Andonov, F. Greco, E. Zhuleku, Observations from the 26th November 2019 Albania earthquake: the earthquake engineering field investigation team (EEFIT) mission, Bull. Earthq. Eng. 19 (5) (2021) 2013–2044.

[39] M.R. Whitworth, G. Giardina, C. Penney, L. Di Sarno, K. Adams, T. Kijewski-Correa, J. Black, F. Foroughnia, V. Macchiarulo, P. Milillo, M. Ojaghi, Lessons for remote post-earthquake reconnaissance from the 14 August 2021 Haiti earthquake, Frontiers in Built Environment 8 (2022) 873212.

[40] B. Voelker, P. Milillo, A. Tavakkoliestahbanati, V. Macchiarulo, G. Giardina, M. Recla, M. Schmitt, M. Cescon, Y.D. Aktas, E. So, The EEFIT remote sensing reconnaissance mission for the February 2023 Turkey earthquakes, IEEE J. Sel. Top. Appl. Earth Obs. Remote Sens. 17 (2024) 19160–19173.

[41] G. Giardina, V. Macchiarulo, F. Foroughnia, J.N. Jones, M.R. Whitworth, B. Voelker, P. Milillo, C. Penney, K. Adams, T. Kijewski-Correa, Combining remote sensing techniques and field surveys for post-earthquake reconnaissance missions, Bull. Earthq. Eng. 22 (7) (2024) 3415–3439.

[42] B. Voelker, P. Milillo, A. Tavakkoliestahbanati, V. Macchiarulo, G. Giardina, M. Recla, M. Schmitt, M. Cescon, Y.D. Aktas, E. So, The EEFIT remote sensing reconnaissance mission for the February 2023 Turkey earthquakes, IEEE J. Sel. Top. Appl. Earth Obs. Remote Sens. 17 (2024) 19160–19173.

[43] V.I. Novelli, R. De Risi, I. Ngoma, I. Kafodya, P. Kloukinas, J. Macdonald, K. Goda, Fragility curves for non-engineered masonry buildings in developing countries derived from real data based on structural surveys and laboratory tests: VI Novelli et al, Soft Comput. 25 (8) (2021) 6113–6138.

[44] V.I. Novelli, D. D'Ayala, N. Makhloufi, D. Benouar, A. Zekagh, A procedure for the identification of the seismic vulnerability at territorial scale. Application to the Casbah of Algiers, Bull. Earthq. Eng. 13 (1) (2015) 177–202.

[45] V.I. Novelli, D. D'Ayala, Assessment of the most damaged historic centres of the Region Emilia Romagna due to the earthquake of the 20th and 29th of May 2012, Ingegneria Sismica 29 (2–3) (2012) 59–71.

[46] Haut-Commissariat au Plan (HCP), Recensement Général de la Population et de l'Habitat 2024 (RGPH 2024): résultats Détaillés, Royaume du Maroc (2024). https://www.hcp.ma/Recensement-general-RGPH_r518.html.
[47] RPS2000, Règlement De Construction Parasismique. Ministère de L'Habitat, de l'Urbanisme et de l'Aménagement de l'Espace, Rabat, Morocco, 2011. Available in French at: https://www.mhpv.gov.ma/wp-content/uploads/2023/10/Guide-RPS-2011-V2011-Francais.pdf.
[48] G. Grünthal, European Macroseismic Scale 1998 (EMS–98), European Seismological Commission, 1998.
[49] Z. Khalil, EEFIT-UM6P workshop. Lessons learned from Al Haouz earthquake: challenges and future strategies, SECED Newsletter 36 (3) (2025). November 2025. ISSN 2517-8008. THE SOCIETY FOR EARTHQUAKE AND CIVIL ENGINEERING DYNAMICS.
[50] T.E. Cherkaoui, A. El Hassani, Seismicity and Seismic hazard in Morocco, Bulletin de l'Institut Scientifique, Rabat, section Sciences de la Terre 34 (2012) 45–55.
[51] M. Sébrier, L. Siame, E.M. Zouine, T. Winter, Y. Missenard, P. Leturmy, Active tectonics in the Moroccan High Atlas, C. R. Geosci. 338 (1–2) (2006) 65–79.
[52] T.S. Irmak, T. Taymaz, M. Palo, S. Yolsal-Çevikbilen, C. Erman, B. Özkan, N. Jabour, T. Eken, Source characteristics and rupture process of the 8 September 2023 M_w 6.8 Al Haouz, Morocco, NW Africa earthquake: insights from multi-scale seismological analysis, Tectonophysics (2026) 231174.
[53] San Fernando Royal Naval Observatory (ROA); Universidad Complutense de Madrid (UCM); Helmholtz-Zentrum Potsdam Deutsches GeoForschungsZentrum (GFZ); Universidade de Évora (UEVORA, Portugal); Institute Scientifique of Rabat (ISRABAT, Morocco), The Western Mediterranean BB Seismic Network, GFZ Data Services, 1996, https://doi.org/10.14470/JZ581150. Dataset/Seismic Network.
[54] C. Rajaram, J.P. Vemuri, A. Bhalkikar, Estimation of Ground Motion Characteristics of the September 08, 2023 Morocco Earthquake, Natural Hazards Research, 2025.
[55] X. Shao, S. Ma, C. Xu, P. Zhang, B. Wen, Y. Tian, Q. Zhou, Y. Cui, Planet image-based inventorying and machine learning-based susceptibility mapping for the landslides triggered by the 2018 M_w 6.6 Tomakomai, Japan Earthquake, Remote Sens. 11 (8) (2019) 978.
[56] D. Zekkos, M. Clark, M. Whitworth, W. Greenwood, A.J. West, K. Roback, G. Li, D. Chamlagain, J. Manousakis, P. Quackenbush, W. Medwedeff, Observations of landslides caused by the April 2015 Gorkha, Nepal, earthquake based on land, UAV, and satellite reconnaissance, Earthq. Spectra 33 (1_suppl) (2017) 95–114.
[57] A. Teixell, M.L. Arboleya, M. Julivert, M. Charroud, Tectonic shortening and topography in the central High Atlas (Morocco), Tectonics 22 (5) (2003).
[58] D.K. Keefer, Landslides caused by earthquakes, GSA Bulletin 95 (4) (1984) 406–421.
[59] H. Tanyaş, C.J. van Westen, K.E. Allstadt, R.W. Jibson, Factors controlling landslide frequency–area distributions, Earth Surf. Process. Landf. 44 (4) (2019) 900–917.
[60] GADM, Download GADM data (version 4.1), Shapefile [Online], https://gadm.org/, 2025.
[61] A.S. Nur, M.F. Fadhillah, Y.H. Jung, B.H. Nam, Y.J. Kim, Y.C. Park, C.W. Lee, Damage proxy map over collapsed structure in Ansan using COSMO–SkyMed data, J. Eng. Geol. 32 (3) (2022) 363–376.
[62] UNESCO World Heritage Centre (n.d.). Morocco: Ksar of ait-ben-haddou. UNESCO World Heritage Convention. Available at: https://whc.unesco.org/en/list/444/.
[63] S.H. Yun, E.J. Fielding, F.H. Webb, M. Simons, Damage Proxy Map from Interferometric Synthetic Aperture Radar Coherence, 2012. USA, Patent No. US9207318B2.
[64] E.J. Fielding, M. Talebian, P.A. Rosen, H. Nazari, J.A. Jackson, M. Ghorashi, R. Walker, Surface ruptures and building damage of the 2003 Bam, Iran, earthquake mapped by satellite synthetic aperture radar interferometric correlation, J. Geophys. Res. 110 (2005) B03302.
[65] E.J. Fielding, J. Jung, Damage Proxy Mapping with SAR interferometric coherence change, Procedia Comput. Sci. 239 (2024) 2322–2328.
[66] R. Natsuaki, H. Nagai, N. Tomii, T. Tadono, Sensitivity and limitation in damage detection for individual buildings using InSAR coherence: a case study in 2016 Kumamoto earthquakes, Remote Sens. 10 (2) (2018) 245.
[67] O.L. Stephenson, T. Köhne, E. Zhan, B.E. Cahill, S.H. Yun, Z.E. Ross, M. Simons, Deep learning–based damage mapping with InSAR coherence time series, IEEE Trans. Geosci. Rem. Sens. 60 (2022) 1–17.
[68] E. Ainscoe, R. Swaminathan, L. Way, Earthquake damage mapped more comprehensively and accurately by radar satellites than optical imagery, Commun. Earth Environ. 6 (2025) 631.
[69] JPL, ARIA share [Online], https://aria–share.jpl.nasa.gov/, 2025. (Accessed 25 August 2025).
[70] EOS–RS, Earth Observatory of Singapore, 2025 [Online], https://sf.earthobservatory.sg/event/EOS-RS_202309_Morocco_Earthquake.
[71] USGS, Landsat project documents [Online], https://www.usgs.gov/landsat–missions/landsat–project–documents, 2025. (Accessed 25 August 2025).
[72] J. Pan, R. Zhao, Z. Xu, Z. Cai, Y. Yuan, Quantitative estimation of sentinel-1A interferometric decorrelation using vegetation index, Front. Earth Sci. 10 (2022) 1016491.
[73] M.O. Román, et al., Satellite–based assessment of electricity restoration efforts in Puerto Rico after Hurricane Maria, PLoS One 14 (6) (2019).
[74] C. Werner, U. Wegmüller, T. Strozzi, A. Wiesmann, Gamma SAR and Interferometric Processing Software, ERS - ENVISAT Symposium, Gothenburg, Sweden, 2000, pp. 16–20. Oct. 2000.
[75] A. Pechnikov, Mobigroup/gmtsar: Pygmtsar–V2023.3.11 [Online], https://zenodo.org/records/7725132, 2023. (Accessed 25 August 2025).
[76] M.O. Román, et al., NASA's black marble nighttime lights product suite, Rem. Sens. Environ. 210 (2018) 113–143.
[77] R. Meli, S. Brzev, M. Astroza, T. Boen, F. Crisafulli, J. Dai, L. Yamin, et al., Seismic design guide for low-rise confined masonry buildings, Confined Masonry Network (2011). Available from: https://www.confinedmasonry.org/wp-content/uploads/2009/09/FINAL_Conf_Mas_Jan_2011.pdf.
[78] SENCICO, Reglamento Nacional de Edificaciones. Norma Técnica E.070: Albañilería, Servicio Nacional de Capacitación para la Industria de la Construcción, Lima, Peru, 2020.
[79] AIS (Asociación Colombiana de Ingeniería Sísmica), NSR-10: Reglamento Colombiano de Construcción Sismo Resistente, 2010. Título D – Mampostería Estructural. Bogotá, Colombia.
[80] Instituto Nacional de Normalización (INN), NCh2123.Of1997 Modificada 2003. Albañilería Confinada—Requisitos Para el Diseño y Cálculo, 2003. Santiago, Chile.
[81] B. Borah, H.B. Kaushik, V. Singhal, Analysis and design of confined masonry structures: review and future research directions, Buildings 13 (5) (2023) 1282.
[82] E. Baglioni, L. Rovero, U. Tonietti, The Moroccan Drâa valley earthen architecture: pathology and intervention criteria, Rammed Earth Conservation (2012) 21–23.
[83] J. Ortega, G. Vasconcelos, H. Rodrigues, M. Correia, Assessment of the influence of horizontal diaphragms on the seismic performance of vernacular buildings, Bull. Earthq. Eng. 16 (9) (2018) 3871–3904.
[84] U. Barbisan, F. Laner, Wooden floors: part of historical antiseismic building systems, Ann. Geophys. 38 (5–6) (1995).
[85] F. Fratini, E. Baglioni, The materials utilised in the earthen buildings sited in the Drâa Valley (Morocco): mineralogical and mechanical characteristics, in: *In Terra Em Seminário*, Lisbõa, Portugal, Argumentum, 2010.
[86] E. Baglioni, F. Fratini, L. Rovero, The characteristics of the earthen materials of the Drâa valley's architecture, J. Mater. Environ. Sci. 7 (10) (2016) 3538–3547.
[87] E. Baglioni, L. Rovero, U. Tonietti, Drâa valley earthen architecture: construction techniques, pathology and intervention criteria, J. Mater. Environ. Sci. 7 (10) (2016) 3499–3508.
[88] B. Khaloufi, The Use of Natural Resources for Housing in Rural Areas of Morocco, 1956.
[89] N. Rabbat (Ed.), The Courtyard House: from Cultural Reference to Universal Relevance, Routledge, 2017.
[90] A. Belabid, H. Akhzouz, H. Elminor, H. Elminor, Monolithic structure technology: a new construction process to enhance traditional construction, International Journal of Sustainable Construction Engineering and Technology 14 (1) (2023) 42–47.
[91] F. Di Michele, E. Spacone, G. Camata, G. Brando, A. Sextos, A. Crewe, H. Varum, Shaking table test and numerical analyses of a full scale three–leaf masonry wall, Bull. Earthq. Eng. 21 (10) (2023) 5041–5081.
[92] A. Giuffrè, Restauro strutturale. Il Rilievo Quale Indispensabile Preliminare Del"Analisi Meccanica, 1993.
[93] M. Corradi, A. Borri, E. Poverello, G. Castori, The use of transverse connectors as reinforcement of multi–leaf walls, Mater. Struct. 50 (2) (2017) 114.

[94] V.I. Novelli, D. D'Ayala, Use of the knowledge–based system LOG–IDEAH to assess failure modes of masonry buildings, damaged by L'Aquila earthquake in 2009, Frontiers in Built Environment 5 (2019) 95.
[95] UN–Habitat, SDG Indicator 11.1.1 Training Module: Adequate Housing and Slum Upgrading, United Nations Human Settlement Programme (UN–Habitat), Nairobi, 2018.
[96] P. Jones, The shaping of form and structure in informal settlements: a case study of order and rules in Lebak Siliwangi, Bandung, Indonesia, Journal of Regional and City Planning 30 (1) (2019) 43–61.
[97] B.W. Wekesa, G.S. Steyn, F.F. Otieno, A review of physical and socio–economic characteristics and intervention approaches of informal settlements, Habitat Int. 35 (2) (2011) 238–245.
[98] O. Bensouda, I.M. Benkirane, V. Becue, J. Cenci, Adaptive housing mechanisms within resettlement sites: a case study of Ouled M'Barek resettlement program, Kenitra, Morocco. Urban, Planning and Transport Research 12 (1) (2024) 2304595.
[99] ICOMOS, Principles for the Analysis, Conservation and Structural Restoration of Architectural Heritage, International Council on Monuments and Sites (ICOMOS), 2003 prepared by the International Scientific Committee for the Analysis and Restoration of Structures of Architectural Heritage (ISCARSAH).
[100] A. Lluveras–Tenorio, A. Andreotti, A. Boujamid, et al., Characterization of the artist's palette from the polychrome decorations of the El Bahia palace doors (Marrakesh, Morocco), J. Cult. Herit. 33 (2018) 213–221.
[101] A. Mesbah, J.C. Morel, J.M. Gentilleau, M. Olivier, Solutions techniques pour la restauration des remparts de Taroudannt (Maroc), in: Terra 2000: 8Th International Conference on the Study and Conservation of Earthen Architecture, Torquay, Devon, UK, May 2000: Preprints, James & James, London, 2000, pp. 266–271.